Electrostatics in soft matter

2009 J. Phys.: Condens. Matter 21 113102

(http://iopscience.iop.org/0953-8984/21/11/113102)

J. Phys.: Condens. Matter **21** (2009) 199801 (1pp) doi:10.1088/0953-8984/21/19/199801

Corrigendum

Electrostatics in soft matter
René Messina 2009 *J. Phys.: Condens. Matter* **21** 113102

It has come to the attention of the author that in the above article a number of errors occurred.

- There is a mistake in the first paragraph on page 4. It should read $e\beta\psi < 1$ instead of $e\psi < 1$, so that it is dimensionless.
- On page 4, in section 2.2.1, both occurrences of reference [17] should read [12,13].
- Further to this the following references are corrected as
  [116] Cherstvy A G and Winkler R G 2006 *J. Chem. Phys.* **125** 064904
  [117] Winkler R G and Cherstvy A G 2007 *J. Phys. Chem.* B **111** 8486–93
  [164] Assoud L, Messina R and Löwen H 2007 *Europhys. Lett.* **80** 48001

J. Phys.: Condens. Matter **21** (2009) 113102 (18pp) doi:10.1088/0953-8984/21/11/113102

TOPICAL REVIEW

Electrostatics in soft matter

René Messina

Institut für Theoretische Physik II, Heinrich-Heine-Universität Düsseldorf, Universitätsstraße 1, D-40225 Düsseldorf, Germany

E-mail: messina@thphy.uni-duesseldorf.de

Received 27 November 2008
Published 17 February 2009
Online at stacks.iop.org/JPhysCM/21/113102

Abstract

Recent progress in understanding the effect of electrostatics in soft matter is presented. A vast number of materials contain ions, ranging from the molecular scale (e.g. electrolyte) to the meso/macroscopic one (e.g. charged colloidal particles or polyelectrolytes). Their (micro)structure and physico-chemical properties are especially dictated by the famous and redoubtable long-ranged Coulomb interaction. In particular, theoretical and simulational aspects, including the experimental motivations, will be discussed.

(Some figures in this article are in colour only in the electronic version)

Contents

1. Introduction

Probably one of the best known and understood ionic materials is sodium chloride (NaCl). In its *solid* form (i.e. NaCl cubic-like crystalline lattice), the experimentally measured heat of vaporization (7.92 eV) can be deduced (within about 10%) from a straightforward lattice sum of the form[1]

$$E_{\mathrm{M}} = \frac{e^2}{4\pi\epsilon_0} \sum_{\text{lattice}} \frac{\alpha_j}{|\vec{r}_j|} \simeq -1.747 \frac{e^2}{4\pi\epsilon_0 a_{\mathrm{L}}} \qquad (1)$$

leading to the theoretical Madelung energy (here $E_{\mathrm{M}} = -8.94$ eV) [1, 2]. This striking good agreement demonstrates that electrostatics is indeed the relevant ingredient governing this ionic crystal [3]. In its *liquid* form, NaCl plays a fundamental role in soft matter, since it controls the degree of screening of the Coulomb interaction in all water based solutions. It is exactly this type of problem that this review will address: electrostatics in soft matter.

Virtually all materials are more or less charged at the mesoscopic scale, depending on the degree of polarizability of the embedding solvent (or matrix) and the solute particles (e.g. colloidal particles, polymers, membranes, etc). The best known example of a polar solvent is evidently water, which plays a crucial role in life and in biological processes as well as in industrial applications. When macroscopic solute particles are polar too, they can then dissociate into charged particles (also called *macroions*) and (*microscopic*) counterions. The counterion distribution near macroions turns out to be decisive for the surface properties of the macroion.

[1] The resulting energy in equation (1) corresponds to the cohesive energy per NaCl molecule. An ion (either Na^+ or Cl^-) is placed at the origin and $\alpha_j = +1, -1$ depending on the type of ion sitting at the lattice site $\vec{r}_j$. $e = 1.602 \times 10^{-19}$ C stands for the usual elementary charge, $\epsilon_0 = 8.854 \times 10^{-12}$ F m^{-1} for the vacuum permittivity, and $a_{\mathrm{L}} = 2.81$ Å for the NaCl lattice parameter.

The pioneering works of Gouy and Chapman [4, 5], realized almost one century ago, concern the counterion distribution near a planar charged interface. Applying the currently named Poisson–Boltzmann theory, they demonstrated that the counterion distribution profile decays algebraically as a function of the separation from the wall with a characteristic length that is inversely proportional to the surface charge density of the wall. Ten years later, Debye and Hückel [6] accomplished a fundamental advance towards the understanding of screening. This theory, originally developed for electrolytes, i.e. a solution of microscopic cations and anions such as Na^+ and Cl^-, and based on the linearization of the Poisson–Boltzmann equation, is now widely used in plasma and solid state physics[2].

Mean-field theories are appealing tools due to their intuitive and clear physical basis, and are robust theories as long as *electrostatic correlations* are not too important. In many practical situations (chromatin, polyelectrolyte multilayering, charged colloidal suspension, etc) electrostatic correlations are strong enough to cause mean-field theories to fail, even on a qualitative level. Two striking and natural consequences of electrostatic correlations that can not be explained by mean-field theories are charge reversal (also called overcharging) and like-charge attraction: (i) overcharging concerns the situation where a macroion is locally covered by a cloud of counterions whose global charge overcompensates that of the macroion so that the net charge (or effective charge) of the complex changes sign; (ii) like-charge attraction is the counter-intuitive effective attraction between two macroions having the same electric charge sign.

A colloidal suspension, the classical material of soft matter science, can crystallize via a strong enough mutual electrostatic repulsion. An understanding of the resulting phase behavior necessitates approaches where particle–particle correlations must obviously be taken into account. This constitutes another example where approaches going beyond the mean-field level are required.

The present work examines the problem of electrostatics in soft matter systems using simple theoretical models and computer simulations. The role of small counterions is addressed in section 2. The relevance of excluded volume (i.e. the finite hard-core size of the constitutive ions) is discussed in section 3. The problem of image charges as occurring near curved dielectric interfaces is presented in section 4. The basic physics in more complex processes such as polyelectrolyte adsorption and multilayering is elucidated in section 5. Colloidal dispersions in strong confinement are presented in section 6. Finally, a conclusion and a possible outlook are provided in section 7.

2. Electrolyte at interfaces

2.1. Foundations of electrostatic mean-field theories in soft matter

This section deals with the foundations of the electrostatic mean-field theories in soft matter. It is written on a pedagogical level such that the non-specialist reader should be in a position to easily comprehend the underlying physics. Nonetheless, the expert will also certainly find some clarifying ideas in the forthcoming discussion.

[2] Note that a similar potential of interaction (so-called Yukawa potential) arises at the subatomic scale to describe the cohesion of the nuclear matter. Nonetheless, in nuclear physics, the interpretation of this potential in terms of screening is not adequate.

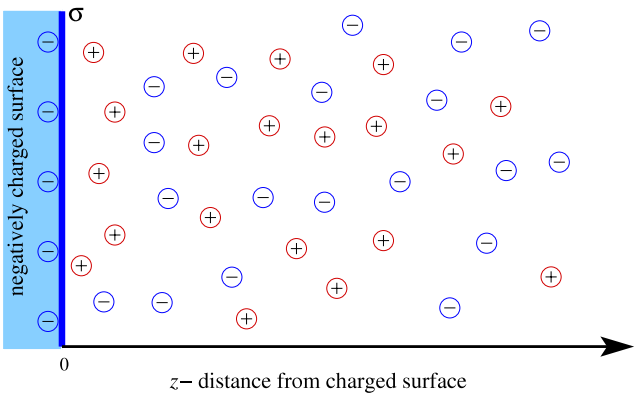

Figure 1. Model for a simple electrolyte near a (negatively) charged surface.

2.1.1. Poisson–Boltzmann theory. The model system we have here in mind is sketched in figure 1. We have to deal with a uniformly charged interface with a surface charge density σ, separating the semi-infinite substrate from a simple electrolyte (consisting of univalent cations (+) and anions (−)) with bulk concentration ρ_0. The system is globally electroneutral and the embedding solvent is merely characterized by its dielectric constant. In this context, the first theoretical determination of counterion distribution for an inhomogeneous fluid was realized independently by Gouy [4] and by Chapman [5] almost a century ago. This mean-field approach corresponding to the so-called Poisson–Boltzmann (PB) theory will now be explained and discussed.

A central quantity in the statistical mechanics of fluids is the *potential of mean force* (PMF). The latter corresponds to the potential stemming from the effective force between two objects. The term 'effective' means here a thermodynamical averaging whose form is dependent on the ensemble (e.g. canonical, grand canonical $\cdots$) under consideration. For the sake of simplicity we will consider the thermodynamical (i.e. macroscopic) limit, where all ensembles are equivalent.

A good starting point is provided by the exact Poisson equation relating the mean electrostatic potential (MEP), $\psi(z)$, to the PMF, $w_\pm(z)$, as follows:

$$\Delta\psi(z) = -\frac{e\rho_0}{\epsilon_0\epsilon_{\rm solv}}\{\exp[-\beta w_+(z)] - \exp[-\beta w_-(z)]\}, \quad (2)$$

where $\epsilon_{\rm solv}$ is the relative permittivity of the solvent (for water $\epsilon_{\rm solv} \approx 80$); $\beta \equiv 1/(k_{\rm B}T)$ the reduced inverse temperature, with $k_{\rm B}$ being the Boltzmann constant and T the absolute temperature. The central approximation of PB theory is to now set

$$w_\pm(z) \overset{\rm (PB)}{\simeq} \pm e\psi(z), \quad (3)$$

such that the exact Poisson equation (2) becomes in the framework of the PB theory

$$\Delta\psi(z) = \frac{2e\rho_0}{\epsilon}\sinh\left[\beta e\psi(z)\right] \qquad (\epsilon \equiv \epsilon_0\epsilon_{\rm solv}) \tag{4}$$

which is the well known PB equation. The resulting MEP, that satisfies the boundary condition $-\frac{\mathrm{d}\psi}{\mathrm{d}z}|_{z=0} = \frac{\sigma}{\epsilon}$, reads [7]

$$\psi(z) = -\frac{2k_{\rm B}T}{e}\ln\left[\frac{1+\gamma\exp(-\kappa z)}{1-\gamma\exp(-\kappa z)}\right], \tag{5}$$

where γ is given by the positive root of

$$\gamma^2 + (2\kappa b)\gamma - 1 = 0 \qquad \text{so that}$$
$$0 \leqslant \gamma = -\kappa b + \sqrt{1+(\kappa b)^2} < 1. \tag{6}$$

We have introduced here in equations (5) and (6) two important length scales, namely the screening length κ^{-1}

$$\kappa^2 \equiv 8\pi\ell_{\rm B}\rho_0 \tag{7}$$

and the Gouy–Chapman length b

$$b \equiv \frac{e}{2\pi\ell_{\rm B}|\sigma|}, \tag{8}$$

where $\ell_{\rm B}$ is a third relevant length in charged soft matter known as the Bjerrum length[3] and reads

$$\ell_{\rm B} \equiv \frac{e^2}{4\pi\epsilon k_{\rm B}T}. \tag{9}$$

The *salt-free* case can be easily obtained by considering the limit $\kappa b \to 0$ in equations (5) and (6). Doing so we find

$$\lim_{\kappa b\to 0}\psi(z) = \frac{2k_{\rm B}T}{e}\ln\left[1+z/b\right] + \frac{2k_{\rm B}T}{e}\ln\frac{\kappa b}{2}. \tag{10}$$

The corresponding counterion distribution, $\rho_+(z) = \rho_0\exp\left[-\beta e\psi(z)\right] = \frac{\kappa^2}{8\pi\ell_{\rm B}}\exp[-\beta e\psi(z)]$, is then merely given by

$$\rho_+(z) = \frac{1}{2\pi\ell_{\rm B}}\frac{1}{(z+b)^2} \qquad \text{(salt-free)}. \tag{11}$$

This formula (11) gives the Gouy–Chapman counterion distribution. The corresponding plot can be found in figure 2.

To better understand the physical meaning involved in the approximation (3), we shall make use of the exact so-called Yvon–Born–Green (YBG) hierarchy [8–10], that reads (taking into account the translational invariance in the (x, y)-plane)

$$-\vec{\nabla}_1 w_\alpha(z_1) = -\frac{q_\alpha|\sigma|}{2\epsilon}\vec{e}_z - \sum_{\beta=1}^{2}\int\vec{\nabla}_1\left[\frac{q_\alpha q_\beta}{4\pi\epsilon r_{12}}\right]g_{\alpha\beta}(r_{12},z_1,z_2)\rho_\beta(z_2)\,\mathrm{d}^3r_2. \tag{12}$$

Equation (12) can be seen as a 'Newtonian' version of the statistical Poisson equation (2). The left-hand side of equation (12) represents the effective force felt by test ion 1 of species $\alpha = \pm$ at the prescribed location $\vec{r}_1 = (x_1, y_1, z_1)$.

[3] The physical interpretation of the Bjerrum length is straightforward: it is the distance between two elementary charges e that leads to an electrostatic interaction equal to $k_{\rm B}T$.

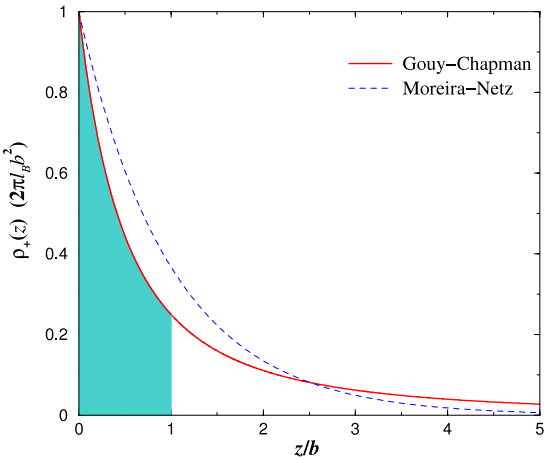

Figure 2. Reduced (Gouy–Chapman) counterion distribution $\rho_+(z)(2\pi\ell_{\rm B}b^2) = \frac{1}{(1+z/b)^2}$ as given by equation (11). It is precisely at $z = b$ that the cumulated counterions (shadowed region) half-compensate the charge of the surface. In other words, the counterion integrated charge at $z = b$ is exactly $-\sigma/2$. The strong Coulomb coupling limit (Moreira–Netz) $\rho_+(z)(2\pi\ell_{\rm B}b^2) = \exp(-z/b)$ as given by equation (19) is also shown for direct comparison.

The right-hand side of equation (12) is made up of two contributions. (i) The first term is merely the Coulomb interaction between the charged interface and test ion 1. (ii) The second term involves the interaction between test ion 1 and the remaining solute ions, with $g_{\alpha\beta}(r_{12}, z_1, z_2)$ (where $r_{12} = |\vec{r}_1 - \vec{r}_2|$) being the pair distribution function and $\rho_\beta(z_2)$ the local ion density. If the former is approximated by $g_{\alpha\beta}(\vec{r}_1, \vec{r}_2) \approx 1$ then equation (12) becomes

$$-\vec{\nabla}_1 w_\alpha(z_1) = -\vec{\nabla}_1\underbrace{\left[q_\alpha\left\{\frac{|\sigma|}{2\epsilon}z_1 + \sum_{\beta=1}^{2}\int\frac{q_\beta}{4\pi\epsilon r_{12}}\rho_\beta(z_2)\,\mathrm{d}^3r_2\right\}\right]}_{=q_\alpha\psi(z_1)}, \tag{13}$$

so that the potential of mean force reduces to the MEP times the charge, which is precisely the PB approximation. In other words, the PB theory neglects the (lateral) *ion–ion correlations* since the condition $g_{\alpha\beta}(\vec{r}_1, \vec{r}_2) = 1$ is required[4]. It is for this reason that the PB theory is a mean-field one. Recalling that

$$g_{\alpha\beta}(r_{12}, z_1, z_2) \equiv \frac{\rho^{(2)}_{\alpha\beta}(r_{12}, z_1, z_2)}{\rho_\alpha(z_1)\rho_\beta(z_2)}, \tag{14}$$

where $\rho^{(2)}_{\alpha\beta}(r_{12}, z_1, z_2)$ is the two-particle density function, one can equally well provide a geometrical interpretation: the probability of finding two ions anywhere in the solution is *independent* of their relative separation in the PB framework[5].

[4] Note that the existence of lateral ion–ion correlations (i.e. $g_{\alpha\beta}(\vec{r}_1, \vec{r}_2) - 1 \neq 0$) has two physical origins: (i) electrostatics and (ii) steric effects due to excluded volume. The latter is implicitly ignored in the PB framework.

[5] Clearly, the bare Coulomb forces between all constitutive ions are properly taken into account in the PB theory, see equation (13). It is the assumption of a structureless lateral arrangement of the ions that creates the crucial inconsistency in the PB framework.

2.1.2. Debye–Hückel theory. In general, the strongly nonlinear PB equation (4) can not be solved analytically, and its linearized version is usually employed instead. This latter approach was historically first developed by Debye and Hückel [6]. When the MEP is everywhere small (i.e., $|e\psi| < 1$), the PB equation reduces to

$$\Delta\psi = \kappa^2\psi \tag{15}$$

and the corresponding solution reads

$$\psi(z) = \psi_S \exp(-\kappa z) = -\frac{2}{\kappa b}\frac{k_B T}{e}\exp(-\kappa z), \tag{16}$$

where ψ_S denotes the surface potential. This result (16) can be obtained either by directly solving the DH equation (15) or substituting the small ψ_S value in the full PB solution equations (5) and (6).

In order to more deeply understand the physical meaning of the linear approximation, we shall rewrite the DH equation (15) in an equivalent integral-equation form. In this context, it is instructive to use an approximate closure for the (exact) Ornstein–Zernike equation, as done by McQuarrie for a bulk electrolyte [11], which leads to the DH description:

$$h_{0\alpha}(z_1) = \underbrace{c_{0\alpha}(z_1)}_{\overset{(DH)}{\approx} -\alpha z_1/b} + \sum_{\beta=1}^{2}\rho_\beta \int h_{0\beta}(z_2)\underbrace{c_{\beta\alpha}(r_{12}, z_1, z_2)}_{\overset{(DH)}{\approx} -\alpha\beta\ell_B/r_{12}} \mathrm{d}^3 r_2 \tag{17}$$

$$= \underbrace{c_{0\alpha}(z_1)}_{\overset{(DH)}{\approx} -\alpha z_1/b} + \sum_{\beta=1}^{2}\rho_\beta \int \underbrace{c_{0\beta}(z_2)}_{\overset{(DH)}{\approx} -\beta z_2/b} h_{\beta\alpha}(r_{12}, z_1, z_2)\,\mathrm{d}^3 r_2, \tag{18}$$

where the subscript '0' in equations (17) and (18) stands for the charged interface, which can be envisioned as a special particle species at infinite dilution. Thereby, this notation preserves nicely the analogy with the bulk case. The DH theory is readily obtained upon assuming that the direct correlation function is equal to the (sign reversed) reduced pair potential (i.e., $c(r) = -\beta V(r)$), which becomes exact when $\rho_0\ell_B^3 \to 0$ and $b/\ell_B \to \infty$. In practice, it is the first line (17) that is used in fluid theory to solve self-consistently the total correlation function $h_{ij} \equiv g_{ij} - 1$ or the PMF via $h_{ij} \overset{(DH)}{\approx} -\beta w_{ij}$.[6]

For the sake of our discussion, however, it is the second line (18) that turns out to be instructive. Indeed, we see now that in the DH theory the term $g_{\beta\alpha}(\vec{r}_1, \vec{r}_2)$ is not trivially unity, since $h_{\beta\alpha}(\vec{r}_1, \vec{r}_2)$ does not vanish in equation (18),[7] in contrast to what happens in the PB situation. Hence ion–ion correlations are *not* neglected[8]. This might seem at first sight counter-intuitive, since the DH theory is based on the linearization of the PB equation, which ignores lateral correlations. This being said, in the weak Coulomb coupling and dilute regime where the DH theory is supposed to be valid, the deviations from the uncorrelated limit become small.

[6] Note that in the DH theory the same central approximation (equation (3)) holds. This is to say that in both theories (PB equation and its linearized version) the PMF is the MEP times the charge.

[7] The reason why $h_{\beta\alpha}(\vec{r}_1, \vec{r}_2)$ does/can not vanish in equation (18) is clear: if one puts $h_{\beta\alpha}(\vec{r}_1, \vec{r}_2) = 0$ in equation (18), then the MEP would simply be linear in z (i.e. the bare electrostatic potential $\frac{k_B T}{e}\frac{z}{b}$ stemming from the charged surface) instead of the expected exponential decay (due to screening) given by equation (16).

[8] Note that McQuarrie used the very same method (equation (18)) to determine analytically (via Fourier transformation) the DH potential in spherical geometry [11]. However, in the past, he was not aware of the relevance of lateral ion–ion correlations, and therefore did not point out this issue.

2.2. Strong Coulomb coupling

2.2.1. Strong Coulomb coupling theories. This last decade, a remarkable theoretical achievement [12–14] has been accomplished in the other extreme limit of strong Coulomb coupling. More specifically, the counterion distribution near a charged planar wall has been predicted analytically by Shklovskii [13] and Moreira and Netz [14] in the strong Coulomb coupling regime (i.e. the Gouy–Chapman problem at low temperature). A common and essential feature of these two works is that the counterion distribution decays exponentially like $\exp(-z/b)$. These two approaches will be now briefly presented.

- Using a field theoretic formulation applied to charged fluids [15, 16], Moreira and Netz [14] showed that at high Coulomb coupling (i.e. for $\Xi \equiv \frac{\ell_B}{b} \gg 1$) the counterion distribution obeys the following *exact* and elegant limiting law:
$$\frac{\rho(z)}{2\pi\ell_B\sigma_s^2} = \exp(-z/b) \tag{19}$$
with $\sigma_s = |\sigma|/e$ being the number of elementary charges e per unit area. A plot of equation (19) can be found in figure 2, where a convenient comparison with the high-temperature limit (equation (11)) can be made.
- Using a rather different and more intuitive approach, Shklovskii [17] has applied Wigner crystal (WC) concepts [18, 19] to the problem of soft charged matter at an effective low temperature. Using some heuristic but physically sound arguments, essentially based on the simple fact that a 'desorbed' counterion from the (triangular) WC counterion layer is correlated to the hole left behind over the Gouy–Chapman length b, Shklovskii [17] obtains (up to the here important prefactor) the same result (equation (19)) as Netz. Interestingly, if one combines (i) the WC approach that provides the correct exponential decay $\exp(-z/b)$ and (ii) the contact theorem which imposes the prefactor, $2\pi\ell_B\sigma_s^2$ [20][9], then one recovers the exact answer (19).

2.2.2. Overcharging and the Thomson problem. As long as the Coulomb coupling between ions is 'fairly' moderate (which is the case for monovalent ions in aqueous solution), the PB theory [4, 5, 21, 22] and even the DH one [23] describe astonishingly well the ion distribution (and hence the thermodynamical system properties) when compared to computer simulations [8, 24–30], theories going beyond the mean-field PB level [31], and even experiments [32]. Nonetheless, as soon as ion–ion correlations become relevant,

[9] Note that $2\pi\ell_B\sigma_s^2 = \frac{1}{2\pi\ell_B b^2}$, so that the PB theory predicts the exact contact value as well (compare with equation (11)); see figure 2. This is not true, however, for the DH version.

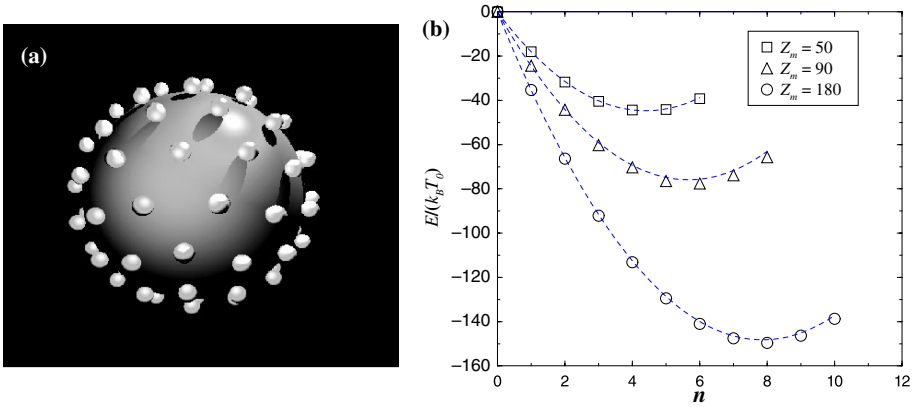

Figure 3. (a) Snapshot of the ground state structure with $Z_m = 180$ corresponding to $N = 90$ counterions. Note the local triangular arrangement on the 'Thomson sphere'. (b) Electrostatic *ground state* energy (in units of k_BT_0 with T_0 being the room temperature) as a function of the number of *overcharging* counterions n for three different bare charges Z_m. The neutral case was chosen as the potential energy origin, and the curves were produced using the theory of equation (22); compare the text. Data taken from [38].

mean-field theories such as the PB one [33, 34] or its linearized version (as related above in section 2.1) cannot explain the experimentally observed relevant effect of overcharging [35, 36] or negative differential capacity [37].

Naively, one would think that the stable configuration corresponds to an exact neutralization of the macroion by the counterions. This assumption is only correct for the case where the counterions are uniformly smeared out over the surface of the colloid. Indeed, basic electrostatics show that, for a central charge $Z_m e < 0$ (representing the macroion) and the shell of radius a of the counterions and (total) charge $Z_c^{(\mathrm{shell})} e > 0$, the electrostatic potential energy is given by [38]

$$E = \frac{Z_m Z_c^{(\mathrm{shell})} e^2}{a} + \frac{Z_c^{(\mathrm{shell})^2} e^2}{2a}, \qquad \text{(CGS)} \qquad (20)$$

where the first term describes the interaction between the central ion and the charged shell and the second one is the electrostatic energy stored in the shell (i.e. the work done upon bringing the counterions from infinity to their current location $r = a$ of the shell). Thereby, the criteria of stability

$$\frac{\partial E}{\partial Z_c^{(\mathrm{shell})}} = 0 \qquad \text{and}$$
$$\frac{\partial^2 E}{\partial Z_c^{(\mathrm{shell})^2}} = e^2/a > 0 \Rightarrow Z_c^{(\mathrm{shell})} = -Z_m \qquad (21)$$

show that the stable configuration corresponds to an exact neutralization. In reality, the counterions are *discrete* and not smeared out, and when electrostatically bound to the macroion's surface they will maximize their separation such as to minimize the counterion–counterion repulsion. This problem turns out to be exactly the one that was addressed a century ago by Thomson [39] (also called the Thomson sphere or the Thomson problem), who studied the ground state energy and structure of N (classical) electrons confined on a sphere (the model of a classical atom). The Thomson problem has only exact solutions for small N and some magic numbers (e.g. $N = 72$ corresponding to the fullerene structure) [40]. Nonetheless, based on Wigner crystal ideas [13, 18, 41], a (discrete) analytical model was developed, which quantitatively accounts for the energy gain upon adsorbing overcharging counterions[10] [38, 42]. More precisely, the following relation for the energy variation ΔE_n (relative to the globally neutral state characterized by $n = 0$ overcharging counterion and $N = Z_m/Z_c$ counterions; see figure 3 for a typical counterion arrangement) as a function of the number n of (excess) overcharging Z_c-valent counterions [38] was derived:

$$\Delta E_n = -\frac{\alpha Z_c^2}{\sqrt{4\pi a^2}}\left[(N+n)^{3/2} - N^{3/2}\right] + \frac{Z_c^2 n^2}{2a}, \qquad \text{(CGS)} \qquad (22)$$

where α (≈ 2) is a numerical geometrical prefactor that was determined by simulations (deduced from the value of ΔE_1).[11] The first, attractive, term in equation (22) stems basically from the interaction between a counterion and its oppositely charged Wigner–Seitz cell. Energy profiles of equation (22) are sketched in figure 3, where one can see that these analytical predictions are pretty robust. This simple approach to the understanding of overcharging via the Thomson problem, Wigner crystal concept and computer simulations has triggered a new interest in the community [43–46] for the Thomson problem applied to soft matter.

We now consider the problem of a pair of macroions. In [42], it was shown that two equally charged spheres are likely to be overcharged and undercharged in the strong Coulomb coupling regime, leading to a metastable *ionized state* that yields a strong long-ranged attraction due to a *monopolar* contribution. All the mechanisms so far reported in the literature can only explain *short-ranged* like-charge attraction [15, 17, 47–57].

[10] To achieve overcharging in nature one should normally add salt to the system to ensure global electroneutrality. For the sake of simplicity, however, we will consider non-neutral systems because they can, on a very simple basis, explain why colloids prefer to be overcharged.

[11] Note that in the case of vanishing curvature (i.e. $a/d_c \to \infty$ where d_c is the mean distance between counterions) our expression becomes exact since the planar WC limit is recovered for which $\alpha = 1.960516\cdots$ [18].

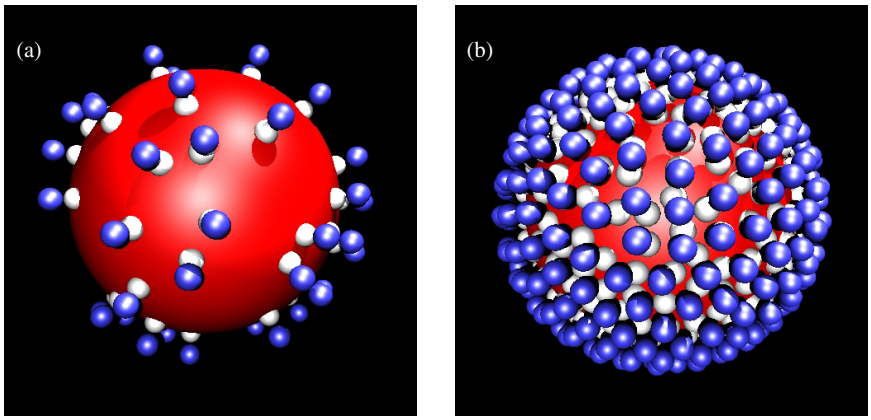

Figure 4. Computer simulation snapshots of counterion ground state configurations. The discrete colloidal surface charges are in white. The counterions are in (dark) blue. (a) 'Low' and (b) 'high' surface charge densities are shown. Data taken from [61].

To further rationalize this phenomenon and the stability of ionized states [38, 58], two charged spheres of the same radius a, carrying the same electric sign of charge but characterized by a charge ratio ρ_Z such that $0 < \rho_Z \equiv Z_B/Z_A \leqslant 1$, were considered. Starting from a macroion pair where each macroion is neutralized by its counterions, the process where a counterion is transfered from macroion B (low bare charge) to macroion A (high bare charge) was investigated [38, 58]. Having demonstrated that the ability of a macroion to become overcharged increases with growing (bare) surface charge density σ (or the bare charge at fixed radius), it is clear that this counterion-transfer process will be energetically favorable below a certain value of ρ_Z. This theoretical prediction shows that the criterion for stable ionized states (the latter also called by other authors [45, 59] 'auto-ionization') is

$$\sqrt{N_A} - \sqrt{N_B} \gtrsim 1 \tag{23}$$

(with $N_{A/B} = Z_{A/B}/Z_c$ being the number of counterions of macroion A/B), which reflects the correlation–hole energy difference between the two macroions (at identical radii). In particular, it was demonstrated that the higher the charge-asymmetry (i.e. ρ_Z) the more stable the ionized state and concomitantly the higher the degree of ionization [38, 58].

The main findings related to this work [38, 42, 58] can be summarized as follows.

- The ground state of a charged sphere is always overcharged due to counterion correlations.
- At finite temperature and in the strong Coulomb regime (accessible with multivalent *aqueous* ions), colloids having different bare surface charge density auto-ionize due to counterion correlations.

2.3. Discretely charged surfaces

The structural (i.e. bare) charge of spherical macroions is usually modeled by a *central* charge, which, by virtue of Gauss' law, is equivalent to a *uniformly* charged macroion surface as far as the electrostatic field (or potential) *outside* the sphere is concerned. However, in nature the charges on the colloidal surface are *discrete* (exactly as the counterions are) and localized; see figure 4. Thus, a natural question that arises is: *why* and *how* does the counterion distribution depend on the way the structural charge of the macroion is represented (i.e. uniformly charged or discrete charges on its surface)? It is precisely this problem that was addressed in [60, 61].

Why is the counterion distribution sensitive to the choice of the representation of the macroion charge (discrete versus uniform)? This question can be best answered by looking at and comparing the (intrinsic) electrostatic potentials generated by discretely and uniformly charged macroions (without counterions) [60]. It was demonstrated in [60] that the electrostatic potential at a reduced distance r/a from the sphere (where a stands for the distance of closest approach between an external unit test-charge and the macroion surface) may be significantly different depending on the nature of the macroion charge. In particular, we show that the higher the bare surface charge (i.e. the closer we get to a uniform charge distribution) the shorter the correlation length (typically $r_c \sim \sqrt{1/\sigma_s}$) between the discrete surface charges, as intuitively expected.

More specifically, the contact potential is sensitive to the localization of the discrete charges, leading to a pronounced depth in their vicinity. All these features, solely based on the spatial behavior of the electrostatic potential stemming from the bare macroion, indicate that the counterion distribution should be much more complicated for a discrete macroion surface charge distribution than for the uniform case.

We now come to the other important question: *how* is the counterion distribution modified when introducing the more realistic discrete macroion's surface charge distribution? This point is thoroughly addressed in [61], where two regimes are considered: ground state ($T = 0$) and finite temperatures. The corresponding relevant findings [60, 61] can be summed up as follows.

- At zero temperature, the counterion (surface) structure possesses greater order the higher the reduced surface charge density σ_s and/or counterion valence Z_c is.
- When overcharging comes into play several scenarios occur: (i) at large σ_s, the overcharging is nearly the same as that obtained at a uniformly charged macroion's surface. (ii) At low σ_s and for *monovalent* counterions,

overcharging is always weaker for discrete macroion charge distribution, due to the ion-pairing frustration for the excess counterions. (iii) At low σ_s and for *highly multivalent* counterions, overcharging can even be stronger in the discrete case due to ion-pairing.

- At finite temperature (in aqueous solutions), the volume counterion distribution is only affected for low σ_s and multivalent counterions.

The effect of surface charge discretization was later examined for different geometries by several groups [62–68].

3. The crucial role of excluded volume

3.1. Effect of electrolyte volume fraction

So far, we have had a pretty good understanding of the physics involved in the counterion distribution for *salt-free* systems where excluded volume effects are irrelevant. The situation becomes much more complicated at finite salt concentrations in aqueous solutions (i.e. water at room temperature in the presence of added salt), where the Coulomb coupling is (rather) weak, especially for monovalent ions. Thereby, a direct application of Wigner crystal ideas is not straightforward enough to account for the unexpected overcharging at *weak* Coulomb coupling that was reported theoretically [69–72], but unexplained, for *monovalent* salt ions of finite size.

Molecular dynamics computer simulations as well as integral-equation theory [73] were employed to identify the mechanisms that govern counterion ordering and overcharging in this weak Coulomb coupling regime. These mechanisms are as follows.

- Increasing the electrolyte particle *size* (at given salt concentration) decreases the available volume of the fluid (or equivalently its entropy) which *favors ion–ion correlations*.
- The interface provided by the macroion causes an increase of the ion density close to it, and concomitantly enhances the *lateral ordering* (similar to the prefreezing phenomenon in *neutral* inhomogeneous fluids).
- Surface lateral ordering and (weak) Coulomb coupling lead to overcharging. These mechanisms are enhanced when dealing with confinement [74, 75].

3.2. Macroion adsorption at planar substrates

Excluded volume effects coupled to electrostatic interactions can also lead to counter-intuitive phenomena in the process of macroion adsorption. A description of the model set-up is sketched in figure 5. For instance, Jimenez-Ángeles and Lozada-Cassou [76] showed, using integral-equation theory, that for moderately (attractive) charged substrates, a film of *coions* first builds up. The electrostatic consequence is that in the direct vicinity of the surface of the substrate its charge becomes amplified (i.e. *surface charge amplification*)[12].

[12] Jimenez-Ángeles and Lozada-Cassou [76] called the phenomenon of surface charge amplification 'overcharging', in contrast to charge reversal that occurs with counterions. Note that charge amplification as well as charge reversal have also been recently reported with the modified Gouy–Chapman theory in [77].

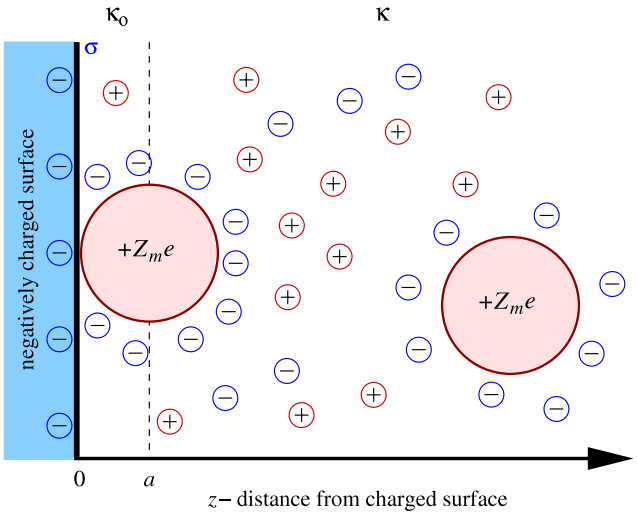

Figure 5. Schematic view of the electrostatic model for macroions near an oppositely charged interface. The macroions are characterized by a distance of closest approach $z = a$ to the charged surface, leading to two screening strengths κ_0 and κ for $0 < z < a$ and $z > a$, respectively.

The driving force of this effect is due to the macroion–ion attractive correlations[13]. This effect was overlooked in the past, because the authors neglected either the finite size of the macroion [78] or the spatial distribution of the small salt ions [79].

Recently, this problem was revisited [80] by using a simple analytical model based on the Debye–Hückel approximation *but* taking into account the finite size of the macroion via its distance of closest approach a (i.e. its radius) to the wall (see figure 5 as well). Two regimes were specifically examined [80]: the strong and weak screening regimes, which are now briefly described.

- In the strong screening regime ($\kappa_0 a \gg 1$) the[14] wall–macroion attractive interaction is exclusively governed by the screening contrast κ_0/κ.[15] More precisely, it was shown that the contact potential of interaction U_m is merely given by

$$\beta U_m \simeq 1 - \frac{\kappa}{\kappa_0}. \tag{24}$$

- In the weak screening regime ($\kappa_0 a \ll 1$) and for sufficiently small surface charge density ($\frac{\kappa b}{2Z_m} \gg 1$), the

[13] The negative counterions of the 'positively charged macroions correspond to the coions of the planar substrate. Thereby, electrostatic correlations tend to localize the counterions of the macroions over *its whole surface* in a uniform manner. Hence, as long as the strength of the surface charge density of the oppositely charged substrate is low enough, a finite number of counterions of the macroions should stay in the vicinity of the interface (see figure 5), leading to a surface charge amplification.

[14] κ_0 stands for the screening strength stemming uniquely from the little ions; see also figure 5.

[15] κ stands for the total screening strength stemming from all the ions present in the solution (also including the macroions); see also figure 5.

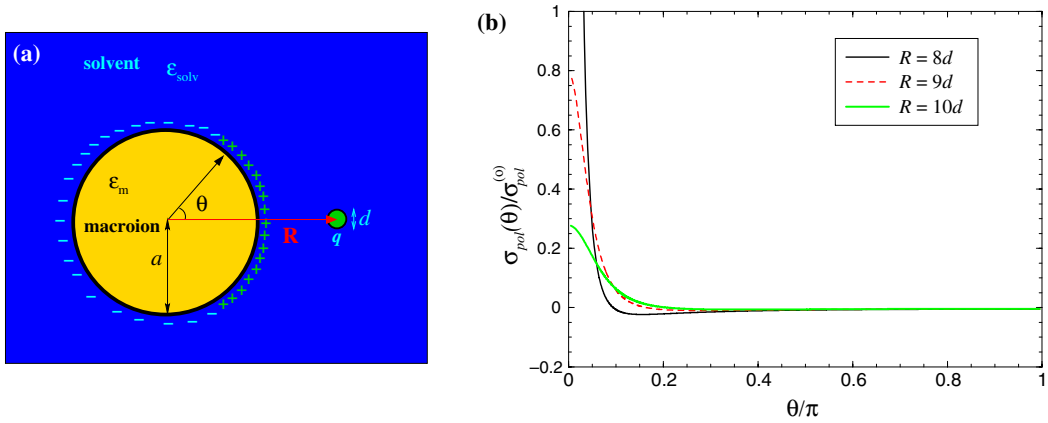

Figure 6. (a) Model for a dielectric sphere (colloid) of dielectric constant ε_m embedded in an infinite medium (the solvent) characterized by a different dielectric constant ε_{solv}. A test positive charge (q) is located near the boundary outside the spherical particle at a radial distance R. The resulting induced surface polarization charges are also illustrated for the case where $\varepsilon_{solv} > \varepsilon_m$. Note that the global induced net charge vanishes. This is a two-dimensional representation of the three-dimensional system. (b) Polar profiles, as obtained from equation (26), of the surface density of polarization charge $\sigma_{pol}^{(sph)}(\theta)$ in units of $\sigma_{pol}^{(0)} = \frac{q}{4\pi\varepsilon_{solv}d^2}$ for different radial distances R of the test-charge q with $\varepsilon_{solv} = 80$, $\varepsilon_m = 2$ and $a = 7.5d$.

reduced electric field[16] at contact follows this simple law:

$$E^*(a) \simeq -\frac{\kappa b}{2Z_m}\left(1 - \frac{\kappa_0^2}{\kappa^2}\right)\kappa a. \qquad (25)$$

This equation (25) tells us that surface charge amplification increases with growing colloidal particle size a and increasing Gouy–Chapman length b (i.e. *decreasing* σ_s).

4. Image charges in spherical geometry

In a typical experimental set-up, the dielectric constant of a macroion is rather low ($\varepsilon_m \approx 2$–5), which is much smaller than that of its embedding solvent (e.g., for water $\varepsilon_{solv} \approx 80$), leading to a *high dielectric contrast*, $\Delta_\varepsilon \equiv \frac{\varepsilon_{solv}-\varepsilon_m}{\varepsilon_{solv}+\varepsilon_m}$, at the interface. It turns out that for a perfect *planar* substrate (which can be envisioned as a colloid of vanishing curvature) there is an elegant analytical solution for the electric field. More precisely, the electric field generated by the induced surface charge at the interface positioned at $z = 0$ (due to the presence of a point-like ion of charge q located at $z = \ell$) can be exactly obtained by a 'fictive' point-like charge $q_{im} = \Delta_\varepsilon q$ located at the mirror position $z = -\ell$ [81]. This feature corresponds to the so-called method of *image charges*. The inclusion of such image forces for the case of an electrolyte close to a planar dielectric interface was studied in the past by computer simulations [62, 82–84], integral-equation formalisms [85, 86], mean-field [78, 87–90] and strong-coupling [62, 91] theories. As far as the cylindrical case [92–94] is concerned, there is no simple 'image charge' picture.

The problem of the dielectric discontinuity in *spherical* geometry is, already at the level of a single ion interacting with a dielectric (neutral) sphere, considerably more complicated than its planar counterpart. Indeed, if we want to reformulate the problem in terms of image charges, one would need an *infinite* number of image charges, thus making its usage much less attractive than in the planar case. Due to this difficulty, the problem of image charges in spherical geometry is sparsely studied in soft matter. Nevertheless, 20 years ago, Linse studied the counterion distribution with image forces around spherical charged micelles by means of Monte Carlo simulations [95]. In his work [95], Linse used a *two-image* charge approximation instead of the full continuous image charge distribution. The conclusions of his study remain qualitatively correct. The dielectric response of a dipolar fluid confined to a spherical cavity was recently addressed by Blaak and Hansen using MD simulations [96].

In the field of image forces in spherical geometry, exact results for the electrostatics of an ion interacting with a dielectric sphere (see figure 6 for the model geometry) were reported [97]. Furthermore, Monte Carlo simulations were performed to elucidate the behavior of an electrolyte near a spherical macroion at finite dielectric contrast, where image forces are properly taken into account [97]. The main results are as follows [97].

- *Single ion.* A compact and exact analytical expression has been derived for the polar profile of the induced surface charge:

$$\sigma_{pol}(\theta) = \frac{q(\varepsilon_{solv} - \varepsilon_m)}{4\pi\varepsilon_{solv}R^2}\sum_{l=1}^{\infty}\left(\frac{a}{R}\right)^{l-1} \times \frac{(2l+1)l}{\varepsilon_{solv}(l+1) + \varepsilon_m l}P_l(\cos\theta), \qquad (26)$$

where q is a test ion at a radial distance R (see figure 6) and P_l designates Legendre polynomials of order l. The *strength* as well as the *range* of image forces in spherical geometry are considerably smaller than at vanishing curvature, due to *auto-screening*.

[16] The reduced electric field is defined as $E^*(z) \equiv -\frac{b}{2}\frac{e}{k_B T}\frac{d\psi(z)}{dz}$ such that at the interface $z = 0$ we have $E^*(0) = -1$.

- *Electrolyte.* For aqueous monovalent ions the (effective) image force is basically equal to the *self-image* one (i.e. the interaction between an ion and its own image). However, when dealing with multivalent counterions, the *lateral* image–counterion correlations can significantly affect the (local) counterion density and, as a major effect, they *screen* the self-image repulsion. Upon adding salt, it was shown that the strength of the image forces induced by the *coions* is marginal. Besides, overcharging is robust against image forces.

Very recently, Reščič and Linse extended [98] the one-colloid problem to the two-colloid interaction problem with a dielectric discontinuity. Using a cylindrical cell model and MC simulations, they found (i) weaker counterion accumulation at the macroion's surfaces, (ii) stronger effective repulsion at moderate Coulomb coupling, and (iii) a less attractive effective force at strong Coulomb coupling. These findings are fully consistent with the one-colloid features just discussed above.

5. Polyelectrolyte adsorption and multilayers

Polyelectrolytes (PEs) are polymers containing a variable (usually large) number of ionizable monomers along the chemical backbone. Once dissolved in a suitable polar solvent such as water, the ion pairs dissociate by creating a charged chain with dissolved counterions. PEs represent a broad and interesting class of materials that have attracted increasing attention in the scientific community. PEs have applications in modern technology as well as in biology, since virtually all proteins, as well as DNA, are charged. The adsorption of PEs onto surfaces is an important process, since they modify the physico-chemical properties of the surface. From a theoretical point of view, charged polymers (in bulk or adsorbed on surfaces) are much less understood [99, 100] than neutral ones [101]. One of the main difficulties is the addition of new length scales set by the tremendously long-ranged Coulomb interaction. Hence, the study of adsorption of PEs is motivated by fundamental aspects as well as practical ones.

5.1. Polyelectrolyte–colloid complexation

5.1.1. Oppositely charged spherical substrates. The works related to the interaction between PEs and *oppositely* charged spheres are briefly reviewed here[17]. The complexation of flexible PEs with oppositely charged macroions is a relevant process in biology [106]. For instance, a nucleosome can be seen as an electrostatic binding between DNA and histone proteins, where the latter can be envisioned as charged spheres[18]. Many theoreticians [104, 107–117] have investigated these types of objects in order to understand the electrostatics governing these structures. Two very relevant results are (i) the possible overcharging of the sphere by long PEs and (ii) a strong wrapping of PEs about the sphere (see figure 7 for an example). A considerable effort has also been provided by simulators [102, 118–129] in the last 12 years.

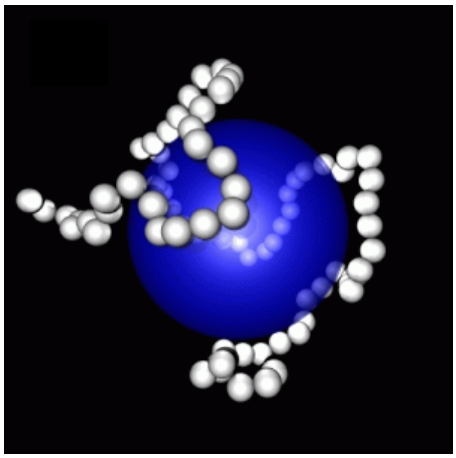

Figure 7. A computer simulation snapshot of PE–colloid complexation (tennis-ball-like conformation) [102].

Some relevant findings in this field can be summarized as follows.

- *The effect of chain stiffness*, which was first systematically studied by Wallin and Linse [118] by MC simulations, is an important key controlling PE adsorption. They showed that the lower the chain stiffness, the higher the PE adsorption, leading to overcharging of the charged sphere by the PE. Stoll and Chodanowski [126], using MC simulation as well but employing electrostatic Yukawa potentials, showed that, upon increasing the chain stiffness, *solenoid* conformations are obtained as predicted analytically by Nguyen and Shklovskii [113].
- *The effect of chain length* has also been addressed (by means of computer simulations) in the past [120, 124, 125, 127]. For a large chain/sphere size ratio, Chodanowski and Stoll [124] found, for fully flexible chains, that only a marginal portion of the PE gets adsorbed to the sphere, and the rest of the chain consists of extended tails. At a 'moderate' chain/sphere size ratio [124], they found strong PE collapse into a tennis-ball-like structure (as illustrated in figure 7). Considering *both* the effects of chain length and the chain stiffness, Akinchina and Linse [127] reported a rich phase behavior: tennis-ball-like, solenoid, multiloop (also called rosette [106]), single loop, as well as 'U'-shaped conformations. Note that there is remarkable agreement with the rosette structure found theoretically by Schiessel *et al* [130].
- The effect of the *discrete* nature of the protein charge distribution was addressed by Carlsson *et al* [131]. In their MC simulations [131], they found that complexation can be stronger with a discrete protein charge distribution (in agreement with the ideas discussed in section 2.3).
- *Multisphere* complexation involving many charged spheres bridged via oppositely charged PEs were investigated by Jonsson and Linse [122, 123] by means of MC simulations. The effect of linear chain charge density, chain length, and macroion charge valency was addressed

[17] The reader can also look at recent reviews [103–105] in this field for more details.

[18] We are aware that this assumption is at best a caricature of a real system (provided that non-specific interactions are dominant). Nonetheless, from an electrostatic viewpoint, we think that the qualitative features should be captured.

in [122]. Interestingly, at prescribed PE linear charge density, the authors found that complexation gets stronger upon increasing the chain length [122]. The effect of chain flexibility was studied in [123], and it was found that the macroion arrangement gradually becomes more linear and ordered along the (long) chain when its stiffness is increased.

5.1.2. Like-charge complexation. Whereas many studies have been devoted to the case of chain–sphere complexation where the two charged bodies are oppositely charged, as we just saw, much less is known concerning the problem of *like-charge sphere–PE complexation*.

In [132, 133], the complexation between a sphere and a long flexible PE (*both negatively charged*) was discussed. Whereas like-charge attraction in the strong Coulomb coupling limit is expected (and therefore complexation too), new and rather unexpected chain conformations are reported. Different coupling regimes as well as the influence of the linear charge density, f, of the PE chain were considered in [133]. The relevant conclusions are as follows.

- At strong coupling the PE chain is always adsorbed as a *flat* structure, whose conformation strongly depends on f. At high f, the conformation consists of densely packed monomers following a Hamiltonian walk. Upon reducing f the chain tends to spread more and more over the particle surface. These findings could have some relevance for organic solutions.
- Under *aqueous* conditions, complexation can be obtained with multivalent counterions and for high enough values of f. In contrast to the strong-coupling case, the formation of *loops* was reported.

5.2. Polyelectrolyte adsorption at planar surfaces

The reader who wants a more detailed account of the field of PE adsorption at surfaces is invited to consult the recent reviews of Netz and Andelman [134] and of Dobrynin and Rubinstein [135]. In this section, we would like to propose some basic ideas and features supported by MC simulations about the adsorption of highly charged polyelectrolytes onto oppositely charged *planar* surfaces in a salt-free environment [136–138]. Flexible [136, 137] as well as rod-like [138] PEs are now discussed.

5.2.1. Role of entropy. There is a simple and clear entropic mechanism that influences *multi-polymer-chain* adsorption that we discuss first. It can be best understood by recalling the *counterion release* effect: the adsorption process of *one* polyion of valence Z typically leads to the release into solution of Z (initially adsorbed) surface monovalent counterions, which is 'electrostatically invariant' but entropically (highly) favorable. *This very same effect is also the reason why longer chains can better adsorb at a prescribed monomer density.* Indeed, at a prescribed monomer density, increasing the chain length N_m involves[19] decreasing the number of chains. Thereby, the resulting (bulk) entropy stemming from the PE chains becomes reduced accordingly. This entropic mechanism linked to the chain length at a prescribed monomer density is henceforth referred to as *polymerization-induced adsorption*.

5.2.2. Flexible chains [136]. When *no* image forces are present (i.e., $\Delta_\epsilon = 0$), it was found that the monomer density profile, $n(z)$, decays monotonically for very short chains even near contact; see figure 8(a). Longer chains experience a short-ranged repulsion in the vicinity of the charged wall ($z \lesssim d$) due to *chain-entropy* effects[20].

When *image forces* come into play, (partial) monomer desorption sets in, whose strength increases with growing chain length N_m. This feature is due to the repulsive image–chain interaction that scales like N_m^2, whereas the attractive Wigner crystal correlations[21] scale only like $N_m^{3/2}$.

The fraction of charge $\sigma^*(z)$ of the fluid as a function of monomer–wall separation, z, is another interesting quantity to characterize the adsorption behavior. At $\Delta_\epsilon = 0$, overcharging (as signaled by $\sigma^*(z) > 1$) occurs as soon as chains are longer than dimers; see figure 4(a) in [136]. In the presence of image forces, the strength of the overcharging is nearly identical to that obtained without image forces at $\Delta_\epsilon = 0$ (compare with figure 4(a) in [137]). Thereby, the main effect of image charges is (i) to decrease the fraction of charge $\sigma^*(z)$ near contact ($z \lesssim 1.2a$) upon growing N_m and (ii) to (slightly) shift the position of the maximum of $\sigma^*(z)$ to larger z.

5.2.3. Rigid chains [138]. Dimers exhibit a monotonic behavior for $n(z)$ that is similar to point-like ions. For longer chains there exists a small monomer depletion near the charged wall for an *intermediate* regime of N_m; see figure 8(a). At high enough N_m, $n(z)$ reveals again a monotonic behavior; see figure 1(a) in [138]. This interesting effect is the result of two antagonistic *entropy* driving forces, namely, (i) chain entropy and (ii) polymerization-induced adsorption. Electrostatic chain–chain correlations, whose strength grows in a non-trivial way with N_m,[22] also favor chain adsorption. Figure 8(a) clearly shows that the adsorption of rigid PEs is much stronger than that of flexible ones. This feature is also detectable in the snapshots; see figures 8(b) and (c).

Upon polarizing the interface, it is found that the degree of adsorption is considerably reduced. Nonetheless, a comparison with the flexible case [137] shows that the values at contact at finite Δ_ϵ are quite similar.

[19] Rigorously, N_m represents the number of monomers per chain corresponding experimentally to the polymerization degree.

[20] The chain-entropy effect here is merely due to the much lower number of available conformations in the adsorbed state. It should be distinguished from that previously discussed in section 5.2.1.

[21] When charged polymers are adsorbed on the surface, they also tend to build a Wigner crystal due to the strong mutual Coulomb interchain repulsion. The higher the chain length N_m (i.e. the length of the chain) the stronger the effect. At prescribed reduced surface charge density σ_s and monomer concentration, this leads to a 2D plasma term (i.e. interchain repulsion reduced by thermal energy) that roughly varies like $N_m^{3/2}$, as is the case for point-like multivalent ions.

[22] Due to the strong extension of the chain, it is no longer suitable to use the point-like and/or spherical polyion picture leading to the WC term in $N_m^{3/2}$.

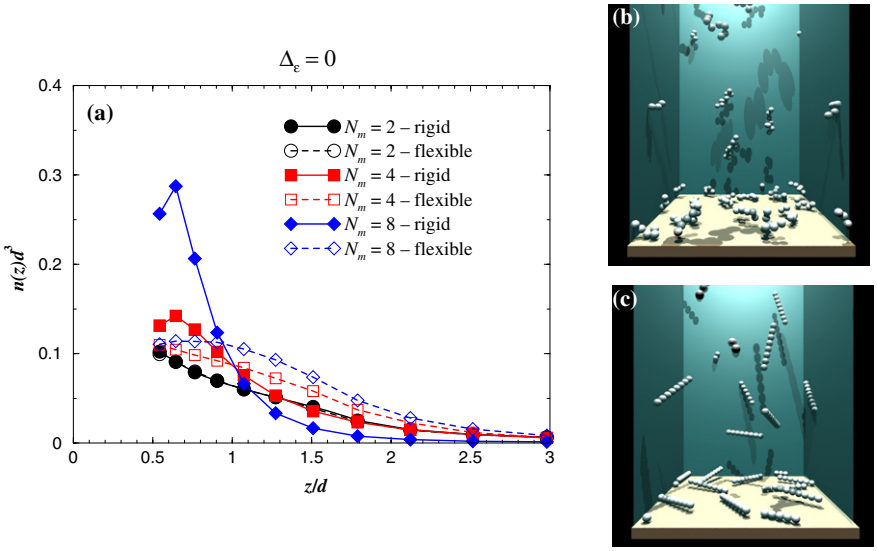

Figure 8. (a) Profiles of the monomer density $n(z)$ for various chain lengths N_m: *flexible* versus *rigid* chains [138]. Snapshots at $N_\mathrm{m} = 8$ for (b) flexible and (c) rigid chains.

5.2.4. Summary. To sum up, MC simulations [136–138] show us the following.

- Without a dielectric discontinuity ($\Delta_\epsilon = 0$), *flexible* PE chains experience short-ranged repulsion near the charged substrate due to chain-entropy effects. In contrast, *rigid* PE chains are more strongly adsorbed (due to a weaker loss of chain-entropy) and, when long enough, experience a purely effective attraction.
- Image forces lower the degree of adsorption for flexible and rigid PE chains. However, the overcharging of the substrate by the PEs is robust (irrespective of the chain flexibility) against image forces.

5.3. Polyelectrolyte multilayering

PE multilayer thin films are often obtained using a so-called layer-by-layer deposition technique [139, 140]: a (say negatively) charged substrate is alternatively exposed to a polycation (PC) solution and a polyanion (PA) one. This method and the resulting materials have a fantastic potential of application in technology, e.g. biosensing [141], catalysis [142], nonlinear optical devices [143], nanoparticle coating [144], etc.

From the theoretical side the literature is rather poor. However, a few analytical works about PE multilayers on charged planar surfaces based on different levels of approximation are available [145–147]. Solis and Olvera de la Cruz considered the conditions under which the spontaneous formation of polyelectrolyte layered structures can be induced by a charged wall [145]. Based on Debye–Hückel approximations for the electrostatic interactions, but including some lateral correlations by the consideration of given adsorbed PE structures, Netz and Joanny [146] found a remarkable stability of the (semi-flexible) PE multilayers supported by scaling laws. For weakly charged flexible polyelectrolytes at high ionic strength, qualitative agreements between theory [147], also based on scaling laws, and experimental observations [148] (such as the predicted thickness and net charge of the PE multilayer) were achieved. More recently, Shafir and Andelman, using mean-field theory, pointed out the relevant role of a specific strong short-range interaction between PAs and PCs.

A tremendous difficulty in PE multilayering is the strong electrostatic correlations between PCs and PAs, which are hard to satisfactorily take into account in (modified) mean-field theories. In this respect, computer simulations are of great help. The first simulation model for PE multilayering was developed in [102]. Later, Panchagnula *et al* performed similar computer simulations [149], where the dynamical aspect was more emphasized. Several types of substrate geometry were considered, from spherical particles [102, 149, 150] to planar substrates [151, 152] via cylindrical ones [153]. Relevant simulation findings for spherical [102] and planar substrates [151] will now be described.

5.3.1. Polyelectrolyte multilayering at spherical substrates. From the study in [102] concerning substrates with finite radii (i.e. charged spheres), one discovers that *non-electrostatic* forces are required to obtain (true) PE multilayers. More precisely, an additional *short-ranged* van der Waals-like attraction (whose strength is characterized by its value at contact, χ_vdw, in units of $k_\mathrm{B}T$) between the substrate's surface and the (monomers of the) oppositely charged chains was considered. The PE structure results then from a complicated interplay between (i) PC–PA strong attraction (favoring a collapse into a compact globular state) and (ii) PE–substrate correlations (favoring *flat* adsorption and *wrapping*[23] around the sphere). Briefly, the main findings in [102] are as follows.

[23] Note that the wrapping of the chain(s) around the colloid is peculiar to spherical substrates. Also it should be noted that wrapping is governed by the repulsive interaction between the turns of a chain [41].

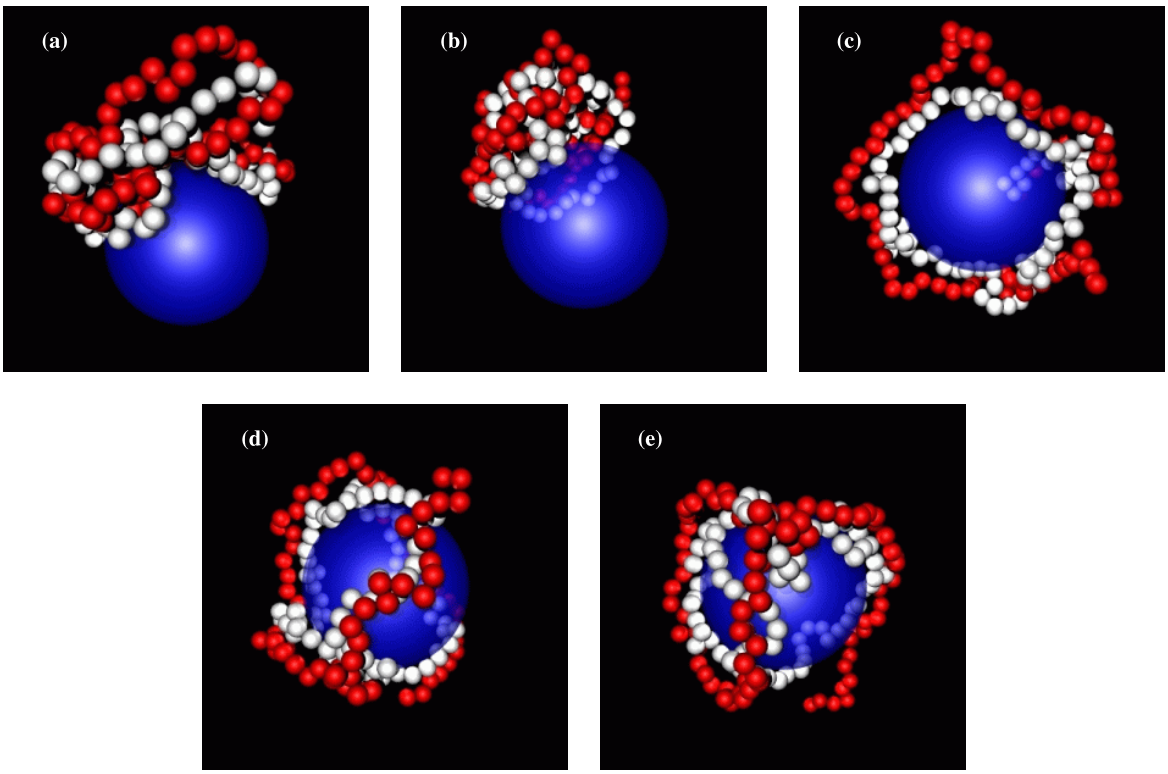

Figure 9. Typical configurations for one PC (in white) and one PA (in (dark) red) adsorbed onto the negatively charged colloid at different χ_{vdw}-couplings. (a) $\chi_{vdw} = 0$, (b) $\chi_{vdw} = 1$, (c) $\chi_{vdw} = 2$, (d) $\chi_{vdw} = 3$, (e) $\chi_{vdw} = 5$. Note the remarkable structural change occurring at $\chi_{vdw} = 2$. The small monovalent counterions (anions and cations) are omitted for clarity.

- Flat *bilayer* structures, involving two long oppositely charged chains, arise only for large enough χ_{vdw}. At low χ_{vdw}, the strong driving PA–PC force leads to PE globular structures; see figure 9.
- Stable and flat multilayers are only obtainable at large enough χ_{vdw}. In a purely electrostatic regime ($\chi_{vdw} = 0$) PE globules are formed, preventing a uniform coverage of the surface; see figure 10.
- Short chains are not suitable candidates for PE multilayers, due to (i) the weaker effect of polymerization adsorption and (ii) reduced chain–chain correlations.

5.3.2. Planar substrates. PE multilayering onto planar substrates was investigated in [151, 152, 154]. The zero-curvature case differs qualitatively from the spherical one. First the intrinsic electric field is higher in the former case[24]. Second the chain wrapping is no longer present at zero curvature. Consequently, at a given surface charge density, we expect a stronger PE layering. The important results can be formulated as follows.

- As with spherical substrates, the relevance of short-ranged non-electrostatic forces is also demonstrated here; see figure 11. Flat multilayers cannot be achieved with solely electrostatic forces.
- The formation of islands (i.e. clusters of PC–PA chains) on a substrate is reported [151] and qualitatively confirms the experimental observations of the early stages of PE deposition (one or two bilayers) [155, 156].

[24] At zero curvature we have $\psi \sim r$, in contrast to finite curvature where $\psi \sim 1/r$.

6. Confined crystalline colloids

It is well known from solid state studies that strongly confined (i.e. quasi-two-dimensional) systems exhibit properties and a phase behavior that may drastically differ from those in the bulk [157]. This feature is also apparent in colloidal systems, and these materials represent ideal model systems to analyze (experimentally as well as theoretically) and to understand confinement effects on a mesoscopic scale corresponding to the interparticle distance. Using external fields, a colloidal system can be prepared in a controlled way into prescribed equilibrium and non-equilibrium states [158]. For instance, in equilibrium, solidification near interfaces (provided by a substrate or a large 'impurity') can occur under thermodynamic conditions where the bulk is still fluid (so-called prefreezing). In non-equilibrium, a wall may act as a center of heterogeneous nucleation (favored by the excess surface energy of the wall/nucleus interface) and thus initiate crystal growth. Most of our experimental knowledge of freezing in a confining slit-like geometry is based on real-space measurements of mesoscopic model systems such as charged colloidal suspensions between glass plates [159, 160].

In this section, different relevant achievements in the field of confined charged colloidal crystals are discussed.

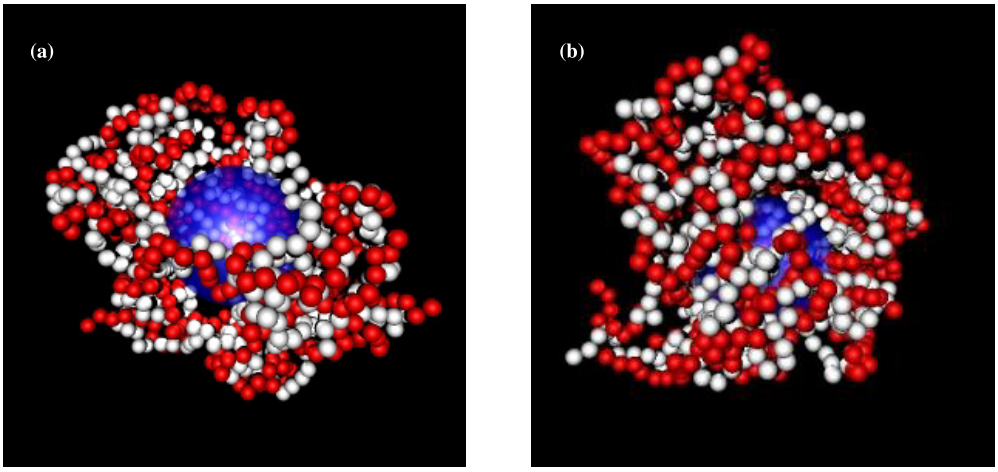

Figure 10. Typical equilibrium configurations for 12 PEs (six PCs in white and six PAs in (dark) red) adsorbed onto the negatively charged colloid at different $\chi_{\rm vdw}$-couplings. Small counterions (anions and cations) are omitted for clarity. (a) $\chi_{\rm vdw} = 0$; (b) $\chi_{\rm vdw} = 3$.

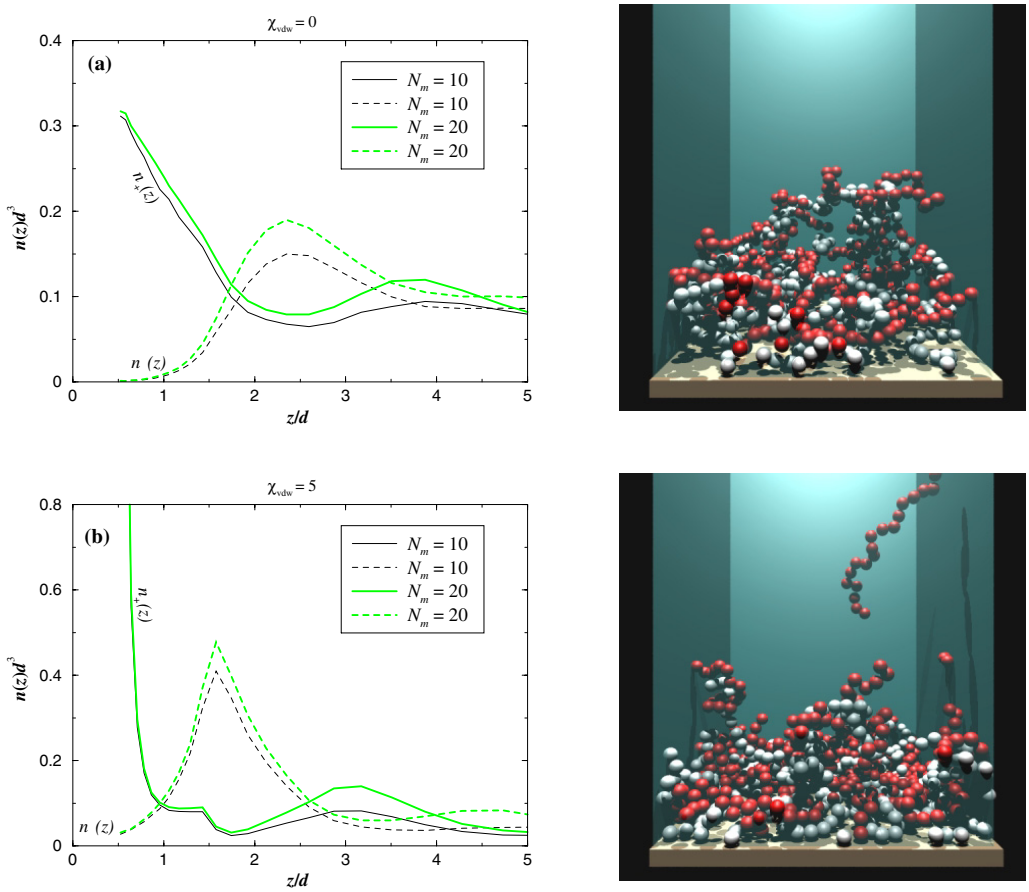

Figure 11. Profiles of monomer density $n_{\pm}(z)$ for oppositely charged PEs adsorbed onto a negatively charged planar substrate. $\chi_{\rm vdw}$-couplings. (a) $\chi_{\rm vdw} = 0$, (b) $\chi_{\rm vdw} = 5$ [151]. The snapshots shown correspond to a chain length $N_{\rm m} = 20$.

6.1. Two-dimensional dipolar mixtures

Two-dimensional colloidal systems can be achieved for instance via sedimentation and trapping at the air/water interface [161, 162]. Applying strong external field, all the dipolar moments align in the direction of the external field, leading to a purely repulsive pair interaction that scales like

$$V_{\rm dip}(r) \propto \frac{m_1 m_2}{r^3}, \qquad (27)$$

where m_1 and m_2 stand for the induced dipolar moments of particles 1 and 2, respectively[25].

[25] Note that in the experimental situations, one has often to deal with *magnetic* colloidal particles (so-called ferrofluids). However *electric* dipoles are also realizable [163]. This being said, regardless of the nature of the dipolar moment (i.e. magnetic or electric), the same pair interaction (27) prevails. Hence results on (super)magnetic particles also fall within the scope of this review.

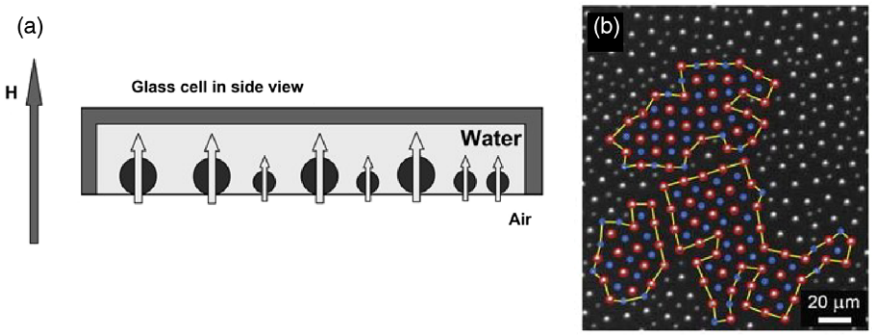

Figure 12. (a) Super-paramagnetic colloidal particles confined at a water/air interface due to gravity. An external magnetic field H perpendicular to the interface induces a magnetic moment $\vec{m}$ in each bead leading to a repulsive dipolar interaction; see equation (27). (b) Micrograph showing three touching square-latticed grains at low reduced temperature with a global composition $X = n_B/(n_B + n_A) \approx 45\%$ (with n_A and n_B denoting the area density of the big and small particles, respectively) and a reduced moment $m_B/m_A \approx 10\%$. Data taken from [162].

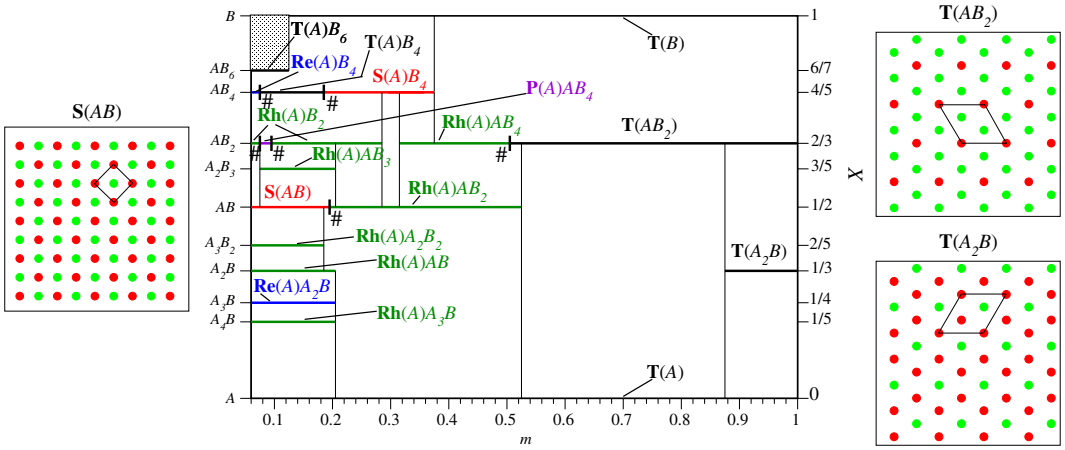

Figure 13. The phase diagram in the (m, X)-plane at $T = 0$. Three important phases are shown: $\mathbf{S}(AB)$, $\mathbf{T}(A_2B)$ and $\mathbf{T}(AB_2)$. The reader can find more details about the other structures in [164]. Data taken from [164].

Whereas the one-component situation trivially yields a triangular lattice, the *binary mixture* situation provides a very rich phase behavior [164]. This feature can be conveniently exploited for potential technological applications: optical band-gap materials (so-called photonic crystals) [165], molecular sieves [166], nano-filters with prescribed porosity [167], etc. There have been recent advances in this field that will be concisely explained here.

Two-dimensional binary mixtures made up of two types of dipolar particles ((i) big particles with a large dipolar moment (species A) and (ii) small particles with a small dipolar moment (species B)) were investigated experimentally [162]. The corresponding set-up and a representative snapshot of the microstructure are shown in figure 12. A remarkable feature is the stability of the square phase at strong dipolar asymmetry ($m_B/m_A \approx 10\%$).

On the theoretical side, the phase behavior of such a binary dipolar mixture at zero temperature was studied using lattice sums [164]. The relevant reduced parameters are (i) the reduced dipolar moment $m = m_B/m_A$ and (ii) the composition $X = n_B/(n_A + n_B)$. The resulting phase diagram is shown in figure 13. The main results are as follows.

- The phase diagram qualitatively differs from that of hard disks [168]. For low dipolar asymmetry $m \gtrsim 0.5$ a stable mixture $\mathbf{T}(AB_2)$ sets in (see figure 13) in contrast to the case of hard-disk mixtures, where *no* mixture is predicted at low size asymmetry [168]. The stability of this phase $\mathbf{T}(AB_2)$ was also reported in molecular dynamics simulations [169]. At even smaller dipolar asymmetry $m \gtrsim 0.88$, an additional (globally triangular) phase mixture $\mathbf{T}(A_2B)$ is stable; see figure 13.
- The stability of the square phase $\mathbf{S}(AB)$ (see figure 13) is in good qualitative agreement with the experimental findings in [162], where the dominance of the square phase is also reported (see figure 12), as previously mentioned.

6.2. *Crystalline colloidal bilayers*

Crystalline bilayers made up of charged particles have been intensively studied in recent years in the soft matter colloid community [170–172] as well as in the solid state physics (classical [173–177] and non-classical electrons [178–180]) and dusty plasma communities [181, 182].

The effective interaction between these constitutive mesoscopic macroions is neither hard-sphere-like nor purely

Coulombic, but it is rather described by an intermediate screened Coulomb (also called Yukawa or DLVO (Derjaguin–Landau–Verwey–Overbeek) [183, 184]) potential due to the screening mediated by the additional microions present in the system. The screening strength can be tuned by varying the microion concentration: for colloidal systems, salt ions can be conveniently added to the aqueous suspension; the dusty plasma, on the other hand, consists of electrons and impurity ions.

6.2.1. Equilibrium. The *equilibrium* phase diagram at zero temperature of crystalline bilayers was investigated theoretically in [170]. The constitutive (point-like) particles interact via a Yukawa pair potential of the form

$$V_{\rm yuk}(r) = V_0 \frac{\exp(-\kappa r)}{\kappa r}, \qquad (28)$$

where V_0 sets the energy scale[26]. The choice of this potential is motivated by the experimental model systems described above. The crystalline bilayer consists of two (identical) layers containing in total N particles in the (x, y) plane. The corresponding (total) surface density ρ is then given by N/A, with A being the (macroscopic) layer area. The distance D, separating the two layers in the z-direction, is prescribed by an (implicit) external potential confining the system.

The zero-temperature phase behavior is fully determined by two dimensionless parameters, namely the reduced layer density, $\eta = \rho D^2/2$, and the reduced screening strength, $\lambda = \kappa D$. Using a straightforward lattice sum technique, the phase diagram was calculated for arbitrary λ and η; see figure 14.[27] The most interesting findings [170] are as follows.

- Whereas the two known extreme limits of zero [173, 175, 176] and infinite [187–189] screening strength λ are recovered by lattice sum calculations [170], it is demonstrated that, at intermediate λ, the phase behavior is strikingly different from a simple interpolation between these two limits. First, there is a first-order coexistence between two different staggered rhombic lattices (IVA and IVB in figure 14) differing in their relative shift of the two unit cells. Second, the staggered rhombic phase IVA exhibits a novel reentrant effect for fixed density and varied screening length; see figure 14. Depending on the density, the reentrant transition can proceed via a staggered square III or a staggered triangular solid V including even a *double reentrant transition* of the rhombic phase IVA, see figure 14.

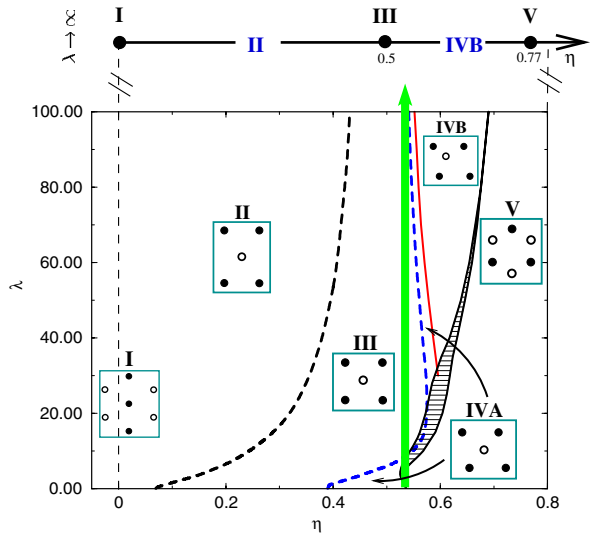

Figure 14. The hard sphere limit $\lambda \to \infty$ is sketched on top. The dashed (solid) lines denote continuous (discontinuous) transitions. The filled region corresponds to the coexistence domain of phases IV and V. The vertical arrow indicates the *double* reentrant behavior of phase IVA. The insets show the lattice geometries, where the filled (open) circles correspond to the lower (upper) layer.

- A comparative study [171] of the phase behavior of highly charged colloidal spheres in a confined wedge geometry reveals semi-quantitative agreement between theory and experiment.

6.2.2. Non-equilibrium. The *non-equilibrium* case[28] at finite temperature as driven by a linear shear flow has been addressed in [190, 191]. The steady state developed under shear as well as the relaxation back to equilibrium after cessation of shear were analyzed with the help of non-equilibrium Brownian dynamics simulations. The pertinent results are the following.

- For increasing shear rates, the following steady states are reported: first, up to a threshold of the shear rate, there is a static solid which is elastically sheared. Then, at higher shear rates the crystalline bilayer melts, and even higher shear rates lead to a reentrant solid stratified in the shear direction.
- After instantaneous cessation of shear, a nonmonotonic behavior of the typical relaxation time is found. In particular, application of high shear rates accelerates the relaxation back to equilibrium since shear-induced ordering facilitates the growth of the equilibrium crystal.
- The orientation of a crystalline bilayer can be tuned at will upon applying a (strong) shear rate in the desired direction and subsequently letting the system relax.

[26] Note that in the ground state, i.e. at zero temperature, the value of V_0 is irrelevant. Nonetheless, in experimental situations, the energy amplitude $V_0 = Z^2\kappa \frac{\exp(2\kappa a)}{4\pi\varepsilon(1+\kappa a)^2}$ scales like the square of the 'effective' charge Z [185, 186]. The latter is typically of the order of 100–100 000 elementary charges such that $V(r = d)$ can be much larger than $k_{\rm B}T$ at average interparticle distances (d), justifying formally our zero-temperature calculations.

[27] Note that the ground state at vanishing screening $\lambda \to 0$ always corresponds to bilayers. Indeed, two equally charged walls do *not* generate any electric field within the slit, and consequently they do not alter the stable Wigner crystal structure obtained at any other surface charge density (including neutral walls). Thereby, if one considers the special case of two walls corresponding to neutralizing backgrounds, the ground state is always a bilayer. At finite screening $\lambda \neq 0$, however, the situation is more complicated, and multilayers (i.e. beyond bilayers) are stable at high enough density η.

[28] The starting unsheared configuration corresponds to a staggered square lattice with a reduced surface particle density $\eta = 0.24$ and a reduced screening strength $\lambda = 2.5$. Two walls are present to ensure the confinement. To this end, screened Coulomb and short-ranged (of the Lennard-Jones type) repulsive potentials were tested, and it was found that our results are marginally sensitive to the choice of the repulsive wall–particle interaction.

7. Conclusions

Various electrostatic effects in soft matter have been discussed. Generally speaking, charged systems are fascinating because they simultaneously involve short-ranged excluded volume effects (as soon as the latter are properly taken into account) already present in neutral systems, and additionally the long-ranged Coulomb interaction. The latter constitutes a formidable theoretical challenge.

In terms of similarities with classical solid state physics and (elementary) quantum chemistry, two striking analogies were identified: (i) the overcharging occurring at a sphere reduces to the old Thomson problem; (ii) the ground state of two spherical macroions is ionized, with the degree of ionization (and therefore the attraction strength) growing with the *difference in surface charge density* between the two macroions. This behavior is highly reminiscent of (molecular) ionic bonding [192], where the *difference in electronegativity* between the two atoms governs its stability.

Excluded volume effects are equally important to fully understand phenomena like overcharging (i.e. surface charge reversal) and surface charge amplification. For overcharging, the counterion layer can reach a high ordering when the local packing fraction is raised by simply increasing the size of the adsorbed counterions.

Image forces turn out to be systematically short ranged. Their effects are only apparent close to the substrate at distances corresponding roughly to the linear size of the microions[29] (counterions and/or charged monomers). As far as the adsorption of polyelectrolytes is concerned, there are two important driving forces that act concomitantly: (i) polymerization-induced adsorption which behaves according to the principle of counterion release (so *entropy* based) and (ii) purely electrostatic lateral correlations (reminiscent of the classical Wigner crystal).

Confined colloidal crystals seem to be now pretty well understood up to bilayers. There is currently some experimental [193, 194] and simulational [195] evidence that, upon increasing the projected surface particle density, the transition from two-layer to three-layer structures involve four (and even more) layered crystalline structures. This is a problem that needs an urgent and clear understanding.

On a more 'material/engineering' level, multilayered structures can apparently be experimentally obtained by combining oppositely charged colloids/micelles [196], instead of polyelectrolytes. To explore this new field, a considerable theoretical effort would be needed to identify the parameters of phase space (such as salt concentration, charges of the colloids and the substrates, particle size etc) allowing the onset of such structures without strong clustering occurring.

Acknowledgments

The author is grateful to C Holm, K Kremer, H Löwen and M Lozada-Cassou, who are closely involved in jointly authored publications covered in this review. It was a pleasure to have fruitful discussions with L Assoud, G He and E Oğuz. A Wynveen is acknowledged for a careful reading of the manuscript.

[29] The behavior might be less clear for highly charged spherical macroions as adsorbate.

References

[1] Madelung E 1918 *Phys. Z.* **19** 542
[2] Ewald P P 1921 *Ann. Phys.* **64** 253
[3] Feynman R P, Leighton R B and Sands M 2006 *The Feynman Lectures on Physics—Mainly Electromagnetism and Matter* Definitive edn, vol 2 (Reading, MA: Addison-Wesley) Chapter 8 (Electrostatic Energy)
[4] Gouy G L 1910 *J. Phys. Radium* **9** 457
[5] Chapman D L 1913 *Phil. Mag.* **25** 475
[6] Debye P and Hückel E 1923 *Phys. Z.* **24** 185
[7] Andelman D 1995 *Electrostatic Properties of Membranes: the Poisson–Boltzmann Theory* (*Handbook of Biological Physics* vol 1) ed R Lipowsky and E Sackman (Amsterdam: Elsevier) chapter 12
[8] Jönsson B, Wennerström H and Halle B 1980 *J. Phys. Chem.* **84** 2179
[9] Carnie S L and Torrie G M 1984 *Adv. Chem. Phys.* **56** 141
[10] Hansen J-P and McDonald I R 2006 *Theory of Simple Liquids* 3rd edn (London: Academic) chapter 4, p 84
[11] McQuarrie D A 1976 *Statistical Mechanics* (New York: Harper and Row) chapter 15, p 345
[12] Perel V I and Shklovskii B I 1999 *Physica* A **274** 446
[13] Shklovskii B I 1999 *Phys. Rev.* E **60** 5802
[14] Moreira A G and Netz R R 2000 *Europhys. Lett.* **52** 705
[15] Netz R R and Orland H 1999 *Europhys. Lett.* **45** 726
[16] Netz R R and Orland H 2000 *Eur. Phys. J.* E **1** 203
[17] Shklovskii B I 1999 *Phys. Rev. Lett.* **82** 3268
[18] Bonsall L and Maradudin A A 1977 *Phys. Rev.* B **15** 1959
[19] Rouzina I and Bloomfield V A 1996 *J. Chem. Phys.* **100** 9977
[20] Wennerström H, Jönsson B and Linse P 1982 *J. Chem. Phys.* **76** 4665
[21] Manning G S 1969 *J. Chem. Phys.* **51** 924
[22] Lebret M and Zimm B H 1984 *Biopolymers* **23** 287
[23] Levin Y and Fisher M E 1996 *Physica* A **225** 164
[24] Linse P, Gunnarsson G and Jönsson B 1982 *J. Phys. Chem.* **86** 413
[25] Lebret M and Zimm B H 1984 *Biopolymers* **23** 271
[26] Deserno M, Holm C and May S 2000 *Macromolecules* **33** 199
[27] Barbosa M C, Deserno M, Holm C and Messina R 2004 *Phys. Rev.* E **69** 051401
[28] Linse P 2005 *Adv. Polym. Sci.* **185** 111
[29] Esztermann A, Messina R and Löwen H 2006 *Europhys. Lett.* **73** 864
[30] Maiti P K and Messina R 2008 *Macromolecules* **41** 5002
[31] Belloni L 1998 *Colloids Surf.* A **140** 227
[32] Bu W, Vaknin D and Travesset A 2006 *Langmuir* **22** 5673
[33] Trizac E and Raimbault J-L 1999 *Phys. Rev.* E **60** 6530
[34] Trizac E 2000 *Phys. Rev.* E **62** R1465
[35] Ruela Talingting M, Voigt U, Munk P and Webber S E 2000 *Macromolecules* **33** 9612
[36] Lin W, Galletto P and Borkovec M 2004 *Langmuir* **20** 7465
[37] González-Tovar E, Jiménez-Ángeles F, Messina R and Lozada-Cassou M 2004 *J. Chem. Phys.* **120** 9782
[38] Messina R, Holm C and Kremer K 2001 *Phys. Rev.* E **64** 021405
[39] Thomson J J 1904 *Phil. Mag.* **7** 237
[40] Wales D J and Ulker S 2006 *Phys. Rev.* B **74** 212101
[41] Grosberg A Y, Nguyen T T and Shklovskii B I 2002 *Rev. Mod. Phys.* **74** 329
[42] Messina R, Holm C and Kremer K 2000 *Phys. Rev. Lett.* **85** 872
[43] Levin Y 2002 *Rep. Prog. Phys.* **65** 1577
[44] Levin Y and Arenzon J J 2002 *Europhys. Lett.* **63** 415

[45] Patra M, Patriarca M and Karttunen M 2003 *Phys. Rev.* E **67** 031402
[46] Mukherjee A K, Schmitz K S and Bhuiyan L B 2003 *Langmuir* **19** 9600
[47] Grønbech-Jensen N, Beardmore K M and Pincus P 1998 *Physica* A **261** 74
[48] Allahyarov E, D'Amico I and Löwen H 1998 *Phys. Rev. Lett.* **81** 1334
[49] Linse P and Lobaskin V 1999 *Phys. Rev. Lett.* **83** 4208
[50] Stevens M J and Robbins M O 1990 *Europhys. Lett.* **12** 81
[51] Lau A W C, Levine D and Pincus P 2000 *Phys. Rev. Lett.* **84** 4116
[52] Grønbech-Jensen N, Mashl R J, Bruinsma R F and Gelbart W M 1997 *Phys. Rev. Lett.* **78** 2477
[53] Ha B Y and Liu A J 1997 *Phys. Rev. Lett.* **79** 1289
[54] Kornyshev A A and Leikin S 1999 *Phys. Rev. Lett.* **82** 4138
[55] Arenzon J J, Stilck J F and Levin Y 1999 *Eur. Phys. J.* B **12** 79
[56] Naji A, Arnold A, Holm C and Netz R R 2004 *Europhys. Lett.* **67** 130
[57] Odriozola G, Jiménez-Ángeles F and Lozada-Cassou M 2006 *Phys. Rev. Lett.* **97** 018102
[58] Messina R, Holm C and Kremer K 2000 *Europhys. Lett.* **51** 461
[59] Mukherjee A K 2003 *J. Phys.: Condens. Matter* **16** 2907
[60] Messina R, Holm C and Kremer K 2001 *Eur. Phys. J.* E **4** 363
[61] Messina R 2002 *Physica* A **308** 59
[62] Moreira A G and Netz R R 2002 *Europhys. Lett.* **57** 911
[63] Lukatsky D B, Safran S A, Lau A W C and Pincus P 2002 *Europhys. Lett.* **58** 785
[64] Allahyarov E, Löwen H, Hansen J P and Louis A A 2003 *Phys. Rev.* E **67** 051404
[65] Henle M L, Santangelo C D, Patel D M and Pincus P A 2004 *Europhys. Lett.* **66** 284
[66] Taboada-Serrano P, Yiacoumi S and Tsouris C 2005 *J. Chem. Phys.* **123** 054703
[67] Qamhieh K and Linse P 2005 *J. Chem. Phys.* **123** 104901
[68] Madurga S *et al* 2007 *J. Chem. Phys.* **126** 234703
[69] Spitzer J J 1983 *J. Colloid Interface Sci.* **92** 198
[70] González-Tovar E, Lozada-Cassou M and Henderson D 1985 *J. Chem. Phys.* **83** 361
[71] Greberg H and Kjellander R 1998 *J. Chem. Phys.* **108** 2940
[72] Deserno M, Jiménez-Ángeles F, Holm C and Lozada-Cassou M 2001 *J. Phys. Chem.* B **105** 10983
[73] Messina R, González-Tovar E, Lozada-Cassou M and Holm C 2002 *Europhys. Lett.* **60** 383
[74] Jiménez-Ángeles F and Lozada-Cassou M 2006 *J. Phys.: Condens. Matter* **18** S2335
[75] Jiménez-Ángeles F and Lozada-Cassou M 2008 *J. Chem. Phys.* **128** 174701
[76] Jiménez-Ángeles F and Lozada-Cassou M 2004 *J. Phys. Chem.* B **108** 1719
[77] Yu J *et al* 2006 *J. Colloid Interface Sci.* **295** 124
[78] Netz R R 1999 *Phys. Rev.* E **60** 3174
[79] Gonzáles-Mozuelos P and Medina-Noyola M 1991 *J. Chem. Phys.* **94** 1480
[80] Messina R 2007 *J. Chem. Phys.* **127** 214901
[81] Jackson J D 1975 *Classical Electrodynamics* (New York: Wiley)
[82] Torrie G M, Valleau J P and Patey G N 1982 *J. Chem. Phys.* **76** 4615
[83] Torrie G M, Valleau J P and Outhwaite C W 1984 *J. Chem. Phys.* **81** 6296
[84] Bratko D, Jönsson B and Wennerström H 1986 *Chem. Phys. Lett.* **128** 449
[85] Kjellander R and Marčelja S 1984 *Chem. Phys. Lett.* **112** 49
[86] Kjellander R and Marčelja S 1985 *J. Chem. Phys.* **82** 2123
[87] Outhwaite C W and Bhuiyan L B 1983 *J. Chem. Soc. Faraday Trans.* II **79** 707
[88] von Grünberg H H and Mbamala E C 2000 *J. Phys.: Condens. Matter* **12** 10349
[89] Sens P and Joanny J-F 2000 *Phys. Rev. Lett.* **84** 4862
[90] Bhuiyan L B, Outhwaite C W, Henderson D and Alawneh M 2007 *Mol. Phys.* **105** 1395
[91] Nguyen T T, Grosberg A Y and Shklovskii B I 2000 *J. Chem. Phys.* **113** 1110
[92] Skolnick J and Fixman M 1978 *Macromolecules* **11** 867
[93] Wynveen A and Bresme F 2006 *J. Chem. Phys.* **124** 104502
[94] Bresme F and Wynveen A 2007 *J. Chem. Phys.* **126** 044501
[95] Linse P 1986 *J. Phys. Chem.* **90** 6821
[96] Blaak R and Hansen J-P 2007 *J. Chem. Phys.* **127** 214901
[97] Messina R 2002 *J. Chem. Phys.* **117** 11062
[98] Reščič J and Linse P 2008 *J. Chem. Phys.* **129** 114505
[99] Barrat J-L and Joanny J-F 1996 *Adv. Chem. Phys.* **94** 1
[100] Joanny J F 2001 *Electrostatic Effects in Soft Matter and Biophysics* vol 46, ed C Holm, P Kékicheff and R Podgornik (Netherlands: Kluwer–Academics) chapter (Scaling Description of Charged Polymers) p 149
[101] de Gennes P G 1979 *Scaling Concepts in Polymer Physics* (Ithaca, NY: Cornell University Press)
[102] Messina R, Holm C and Kremer K 2003 *Langmuir* **19** 4473
[103] Messina R, Holm C and Kremer K 2004 *J. Polym. Sci.* B **42** 3557
[104] de Vries R and Stuart M C 2006 *Curr. Opin. Colloid Interface Sci.* **11** 295
[105] Ulrich S, Seijo M and Stoll S 2006 *Curr. Opin. Colloid Interface Sci.* **11** 268
[106] Schiessel H 2003 *J. Phys.: Condens. Matter* **15** R699
[107] von Goeler F and Muthukumar M 1994 *J. Chem. Phys.* **100** 7796
[108] Gurovitch E and Sens P 1999 *Phys. Rev. Lett.* **82** 339
[109] Mateescu E M, Jeppesen C and Pincus P 1999 *Europhys. Lett.* **46** 493
[110] Park S Y, Bruinsma R F and Gelbart W M 1999 *Europhys. Lett.* **46** 454
[111] Netz R R and Joanny J F 1999 *Macromolecules* **32** 9026
[112] Kunze K-K and Netz R R 2000 *Phys. Rev. Lett.* **85** 4389
[113] Nguyen T T and Shklovskii B I 2001 *Physica* A **293** 324
[114] Schiessel H 2003 *Macromolecules* **36** 3424
[115] Winkler R G and Cherstvy A G 2006 *Phys. Rev. Lett.* **96** 066103
[116] Cherstvy A G and Winkler R G 2007 *J. Chem. Phys.* **125** 064904
[117] Winkler R G and Cherstvy A G 2007 *J. Phys. Chem.* B **111** 5436
[118] Wallin T and Linse P 1996 *Langmuir* **12** 305
[119] Wallin T and Linse P 1996 *J. Phys. Chem.* **100** 17873
[120] Wallin T and Linse P 1997 *J. Phys. Chem.* B **101** 5506
[121] Kong C Y and Muthukumar M 1998 *J. Chem. Phys.* **109** 1522
[122] Jonsson M and Linse P 2001 *J. Chem. Phys.* **115** 3406
[123] Jonsson M and Linse P 2001 *J. Chem. Phys.* **115** 10975
[124] Chodanowski P and Stoll S 2001 *Macromolecules* **34** 2320
[125] Chodanowski P and Stoll S 2001 *J. Chem. Phys.* **115** 4951
[126] Chodanowski P and Stoll S 2002 *Macromolecules* **35** 9556
[127] Akinchina A and Linse P 2002 *Macromolecules* **35** 5183
[128] Dzubiella J, Moreira A G and Pincus P A 2003 *Macromolecules* **36** 1741
[129] Maiti P K and Bagchi B 2006 *Nano Lett.* **6** 2478
[130] Schiessel H, Rudnick J, Bruisma R and Gelbart W M 2000 *Europhys. Lett.* **51** 237
[131] Carlsson F, Linse P and Malmsten M 2001 *J. Phys. Chem.* B **105** 9040
[132] Messina R, Holm C and Kremer K 2002 *Phys. Rev.* E **65** 041805
[133] Messina R, Holm C and Kremer K 2002 *J. Chem. Phys.* **117** 2947
[134] Netz R R and Andelman D 2003 *Phys. Rep.* **380** 1

[135] Dobrynin A V and Rubinstein M 2005 *Prog. Polym. Sci.* **30** 1049
[136] Messina R 2004 *Phys. Rev.* E **70** 051802
[137] Messina R 2006 *Phys. Rev.* E **74** 049906(E)
[138] Messina R 2006 *J. Chem. Phys.* **124** 014705
[139] Decher G, Hong J D and Schmitt J 1992 *Thin Solid Films* **210/211** 831
[140] Decher G 1997 *Science* **277** 1232
[141] Caruso F *et al* 1998 *Langmuir* **14** 4559
[142] Onda M, Ariga K and Kunitake T 1999 *Biosci. Bioeng.* **87** 69
[143] Wu A, Yoo D, Lee J K and Rubner M F 1999 *J. Am. Chem. Soc.* **121** 4883
[144] Caruso F, Caruso R A and Möhwald H 1998 *Science* **282** 1111
[145] Solis F J and de la Cruz M O 1999 *J. Chem. Phys.* **110** 11517
[146] Netz R R and Joanny J F 1999 *Macromolecules* **32** 9013
[147] Castelnovo M and Joanny J F 2000 *Langmuir* **16** 7524
[148] Ladam G *et al* 2000 *Langmuir* **16** 1249
[149] Panchagnula V, Jeon J and Dobrynin A V 2004 *Phys. Rev. Lett.* **93** 037801
[150] Panchagnula V, Jeon J, Rusling J F and Dobrynin A V 2005 *Langmuir* **21** 1118
[151] Messina R 2004 *Macromolecules* **37** 621
[152] Patel P A, Jeon J, Mather P T and Dobrynin A V 2006 *Langmuir* **22** 9994
[153] Messina R 2003 *J. Chem. Phys.* **119** 8133
[154] Patel P A, Jeon J, Mather P T and Dobrynin A V 2005 *Langmuir* **21** 6113
[155] Menchaca J L, Jachimska B, Cuisinier F and Pérez E 2003 *Colloids Surf.* A **222** 185
[156] Harris J J and Bruening M L 2000 *Langmuir* **16** 2006
[157] Binder K 1998 *J. Non-Equilib. Thermodyn.* **23** 1
[158] Löwen H 2001 *J. Phys.: Condens. Matter* **13** R415
[159] Murray C A, Sprenger W O and Wenk R A 1990 *Phys. Rev.* B **42** 688
[160] Neser S, Bechinger C, Leiderer P and Palberg T 1997 *Phys. Rev. Lett.* **79** 2348
[161] Zahn K, Méndez-Alcaraz J M and Maret G 1997 *Phys. Rev. Lett.* **79** 175
[162] Ebert F, Keim P and Maret G 2008 *Eur. Phys. J.* E **26** 161
[163] Yethiraj A and van Blaaderen A 2003 *Nature* **421** 513
[164] Assoud L, Messina R and Löwen H 2007 *Europhys. Lett.* **80** 4801
[165] Blanco A *et al* 2000 *Nature* **405** 437
[166] Kecht J *et al* 2004 *Langmuir* **20** 5271
[167] Yan F and Goedel W A 2004 *Nano Lett.* **4** 1193
[168] Likos C N and Henley C L 1993 *Phil. Mag.* B **68** 85
[169] Stirner T and Sun J 2005 *Langmuir* **21** 6636
[170] Messina R and Löwen H 2003 *Phys. Rev. Lett.* **91** 146101
[171] Barreira Fontecha A *et al* 2005 *J. Phys.: Condens. Matter* **17** S2779
[172] Lobaskin V and Netz R R 2007 *Europhys. Lett.* **77** 38003
[173] Goldoni G and Peeters F M 1998 *Phys. Rev.* B **53** 4591
[174] Partoens B, Schweigert V A and Peeters F M 1997 *Phys. Rev. Lett.* **79** 3990
[175] Schweigert I V, Schweigert V A and Peeters F M 1999 *Phys. Rev.* B **60** 14665
[176] Schweigert I V, Schweigert V A and Peeters F M 1999 *Phys. Rev. Lett.* **82** 5293
[177] Kalman G J, Hartmann P, Donko Z and Golden K I 2007 *Phys. Rev. Lett.* **98** 236801
[178] Świerkowski L, Neilson D and Szymański J 1991 *Phys. Rev. Lett.* **67** 240
[179] Eisenstein J P and MacDonald A H 2004 *Nature* **432** 691
[180] Pereira J M, Vasilopoulos P and Peeters F M 2007 *Nano Lett.* **7** 946
[181] Totsuji H, Kishimoto T and Totsuji C 1997 *Phys. Rev. Lett.* **78** 3113
[182] Zuzic M *et al* 2000 *Phys. Rev. Lett.* **85** 4064
[183] Derjaguin B V and Landau L D 1941 *Acta Physicochim. (USSR)* **14** 633
[184] Verwey E J and Overbeek J T G 1948 *Theory of the Stability of Lyophobic Colloids* (Amsterdam: Elsevier)
[185] Alexander S *et al* 1984 *J. Chem. Phys.* **80** 5776
[186] Bocquet L, Trizac E and Aubuy M 2002 *J. Chem. Phys.* **117** 8138
[187] Pieranski P, Strzelecki L and Pansu B 1983 *Phys. Rev. Lett.* **50** 900
[188] Schmidt M and Löwen H 1996 *Phys. Rev. Lett.* **76** 4552
[189] Schmidt M and Löwen H 1997 *Phys. Rev.* E **55** 7228
[190] Messina R and Löwen H 2006 *Phys. Rev.* E **73** 011405
[191] Löwen H *et al* 2005 *J. Phys.: Condens. Matter* **17** S3379
[192] Pauling L 1939 *The Nature of the Chemical Bond* (Ithaca, NY: Cornell University Press)
[193] Ramiro-Manzano F, Bonet E, Rodriguez I and Meseguer F 2007 *Phys. Rev.* E **76** 050401
[194] Fontecha A B and Schope T P H 2007 *Phys. Rev.* E **76** 050402
[195] Fortini A and Dijkstra M 2006 *J. Phys.: Condens. Matter* **18** L371
[196] Hong J *et al* 2007 *Adv. Mater.* **19** 4364